EXPLORATIONS OF A π-STRIPED, d-WAVE SUPERCONDUCTOR

EXPLORATIONS OF A π-STRIPED, d-WAVE SUPERCONDUCTOR

By J. DAVID BAZAK, B.Sc., B.Sc.F.S.

A Thesis Submitted to the School of Graduate Studies in Partial Fulfillment of the Requirements for the Degree Master of Science

McMaster University MASTER OF SCIENCE (2013) Hamilton, Ontario (Physics)

TITLE: Explorations of a π-Striped, d-Wave Superconductor

AUTHOR: J. David Bazak, B.Sc., B.Sc.F.S. (Trent University)

SUPERVISOR: Professor Catherine Kallin

NUMBER OF PAGES: vii, 72

Abstract

The π-striped, d-wave superconducting (SC) state, which is a type of pair density wave wherein the SC order is spatially modulated, has recently been shown to generate the key ingredients for quantum oscillations consistent with experimental observations (Zelli et al., 2011, 2012). This was accomplished with a phenomenological approach using non-self-consistent Bogoliubov-de Gennes (BdG) theory. The objective of this thesis is to explore two aspects of this approach: the addition of a charge density wave (CDW) order to the previous non-self-consistent calculations, and an attempt at stabilizing the π-striped state in fully self-consistent BdG theory. It was found that the CDW order had a minimal effect on the Fermi surface characteristics of the π-striped state, but that a sufficiently strong CDW degrades the Landau levels which are essential for the formation of quantum oscillations. The self-consistent mean-field calculations were unable to stabilize the π-striped state under a range of modifications to the Hamiltonian. Free energy calculations with the modulated SC order treated as a parameter demonstrate that the π-striped state is always less energetically favourable than the normal state for the scenarios which were considered. The results of this study constitute a basis for future, more comprehensive studies, using the BdG approach, of the stability of possible π-striped SC phases.

Acknowledgements

I would like to sincerely thank my supervisor, Prof. Catherine Kallin, for giving me the opportunity to pursue graduate studies in her research group, and for her patient guidance of my studies. I would also like to thank Profs. John Berlinsky and Erik Sorensen for kindly agreeing to participate in my supervisory committee. Further, my thanks goes to John for acting as my temporary supervisor for several months.

I have had a great experience sharing an office with Sedigh Ghamari and Wen Huang, and thank them for the many wonderful conversations, about physics and otherwise, and for their helpful discussions and suggestions about my research. I would also like to thank my fellow graduate students for the camaraderie and excellent company during my time at McMaster. At the risk of inadvertent omission, I will refrain from trying to list everyone, but in particular I would like to thank Faiyaz Hasan and Jesse Mumford for all of the great times.

Finally, I would like to thank my family for all of the help and support over the years. Most of all, I would like to thank my mother for her guidance, constant encouragement, and unwavering commitment to helping me to achieve my goals. This support has been indispensable in shaping the person that I have become, and I shudder to think where I would be in its absence.

Contents

List of Figures

Chapter 1

Introduction

1.1 An Overview of the Cuprate High-T_c Superconductors

The discovery of the cuprate transition metal oxide high-temperature superconductors (HTS) by Bednorz and Müller (Bednorz and Müller, 1986), and the highly unconventional properties of these materials, has generated a surge of new experimental and theoretical techniques in condensed matter physics (Orenstein and Millis, 2000). These compounds exhibited hitherto unprecedentedly high critical temperatures, T_c – in some cases, above the liquid-air barrier where cooling is accessible with liquid nitrogen (Norman and Pépin, 2003). The parent compounds of these materials are Mott insulators – compounds which have partially filled electron bands that would normally give metallic character, but whose conduction electrons are in fact localized, as in insulators, by strong correlation effects – and the superconducting forms are realized by doping the parent compound with either holes or electrons (Lee et al., 2006). This is in stark contrast to conventional superconductors (SC) described by the Bardeen-Cooper-Schreiffer (BCS) theory, whose parent compounds are elemental metals and alloys (de Gennes, 1966; Tinkham, 2004). Furthermore, these materials have a variety of magnetic phases, and the interplay between magnetism and su-

perconductivity is a key element in cuprate HTS, while they are antithetical in the materials well-described by BCS theory (Basov and Chubukov, 2011). In addition to this, several of the states which lie on the boundary of the SC phase – the pseudogap region and the so-called "strange metal" phase – are also markedly distinct in character from the usual normal state which lies above the SC phase transition.

The general structure of the cuprates consists of stacks of CuO_2 planes, where the Cu atom is fourfold-coordinated with surrounding O atoms, with intervening insulating layers (Norman and Pépin, 2003). They are therefore quasi-two-dimensional materials, and this low-dimensionality, combined with their proximity on the phase diagram to the parent Mott-insulating phase, immediately suggests a fundamental departure from conventional metal physics (Orenstein and Millis, 2000). In the conventional BCS picture, superconductivity arises from an instability of the so-called Fermi sea of electron states with respect to an attractive interaction, leading to the formation of bound states: Cooper pairs (de Gennes, 1966; Tinkham, 2004). Since these pairs are composite bosons, they can propagate without resistance, and because they are formed from electrons in time-reversed states, they have zero centre-of-mass momentum (Norman, 2004). The finite energy necessary to break the Cooper pair manifests as a "gap" in the excitation spectrum, and this gap functions as an order parameter for the SC phase. The generic pairing scenario for the formation of an SC condensate assumes that fermions attract by exchanging quanta of bosonic excitations (Basov and Chubukov, 2011). In the case of BCS theory, these bosons are phonons – quantized vibrations of the crystal lattice. However, in the cuprates the source of this pairing mechanism has stubbornly evaded elucidation. Roughly speaking, two contrasting views exist (Tesanovic, 2011); the more conventional is that the pairing is mediated by (bosonic) spin fluctuations (Basov and Chubukov, 2011; Scalapino, 2012). The alternative view is that the condensate is formed from

a resonating valence bond (RVB) state, which is a spin-liquid from melting of the parent antiferromagnetic (AF) order, and which becomes charged on doping, hence becoming the SC condensate (Norman, 2004).

After much debate, the gap function in the SC phase for the cuprates was determined to have $d_{x^2-y^2}$ symmetry in momentum-space (Tsuei and Kirtley, 2000), which differs from the isotropic s-wave symmetry of the elemental SC. The d-wave symmetry introduces nodes in momentum-space where the gap function changes sign, resulting in locations where zero-energy excitations exist, and therefore has a dramatic impact on the resulting macroscopic properties. In terms of the phase diagram (see, *e.g.*, Damascelli et al. (2003)), the SC region has a dome-like appearance, with the highest T_c occurring at an optimal doping. Increased doping leads to the so-called "overdoped" regime, where the phase boundary is with the strange metal phase, and eventually borders a more conventional Fermi-liquid (*i.e.* "normal metal") phase with higher still doping. On the other hand, decreasing from optimal doping enters the "underdoped" regime, where the SC phase borders the pseudogap region, as well as possible spin glass states and/or states with spatial modulation of the charge and/or spin of the electrons known as density waves (for example, the stripe state discovered by Tranquada et al. (1995), consisting of unidirectional "lanes" of AF order with holes embedded in the domain walls).

The pseudogap phase is particularly controversial, as it has alternately been viewed as a form of order, or a density wave competitor of SC, or a remnant of SC with phase-incoherent Cooper pairs which therefore lacks long-range order (Tesanovic, 2011). It manifests as a gapping of the spin excitations as seen by nuclear magnetic resonance (NMR) experiments (Williams et al., 1997), but has nonzero density of states at the Fermi level (Timusk and Statt, 1999). A further source of intrigue surrounding the pseudogap is the appearance of "Fermi arcs" in momentum-space, as

observed by angle-resolved photoemission spectroscopy (ARPES) (Damascelli et al., 2003). These are line segments of zero-energy excitations centred near the nodal point at $(\pi/2, \pi/2)$ and the four points related by the symmetry of the square-planar CuO_2 layers, which terminate in gaps as these lines approach the $(\pi, 0)$ and $(0, \pi)$ points. The arcs reduce in length with decreasing T, and appear to shrink to the nodal points in the $T \to 0$ limit (Kanigel et al., 2006). The pseudogap has been variously connected with RVB states such as those promulgated by (Anderson, 1987), preformed Cooper pairs as proposed in Randeria et al. (1989), and charge/spin density waves, based on similarities with the observations obtained in Borisenko et al. (2008). In any case, these attributes clearly indicate that the pseudogap is a non-Fermi-liquid state, and its connection with the SC phase where a more conventional quasiparticle picture *does* apply is at the heart of establishing a robust theory of superconductivity in the cuprates.

1.2 Observations of Quantum Oscillations in the Cuprates

One of the key issues surrounding the connection of the various non-Fermi-liquid "normal" states to the SC phase is ascertaining the electronic properties of these states. Determining whether the underdoped cuprates have an underlying Fermi surface, and how its topological character differs from the established Fermi surface in the more conventional overdoped regime, is a crucial aspect of this endeavour (Doiron-Leyraud et al., 2007). In traditional metal physics, one of the most important types of measurements is that of "quantum oscillations" (QO): the observation of oscillatory behaviour as a function of the reciprocal of the magnetic field strength when materials are exposed to strong magnetic fields. The reason is that these oscillations are intimately connected with the Fermi surface, and hence, the electronic properties.

1.2.1 Theory of Quantum Oscillations

The detailed demonstration of the connection between QO and the electronic properties of the material is well-established, and can be found in any standard condensed matter reference text, such as Ashcroft and Mermin (1976). One finds that, since the motion of electrons in a direction perpendicular to a magnetic field is quantized, the area between successive quantized orbits $A(\mathcal{E}_\nu)$ is given by

$$A(\mathcal{E}_{\nu+1}) - A(\mathcal{E}_\nu) \equiv \Delta A = \frac{2\pi H}{\hbar c} \quad \Rightarrow \quad A(\mathcal{E}_\nu) = (\nu + \lambda)\Delta A, \tag{1.1}$$

where λ is the "null" value associated with the lowest Landau level (Onsager, 1952). Equation (1.1) demonstrates that the level spacing ΔA will change in proportion to the magnetic field strength, H. Clearly then, as the field strength is increased, the levels near the Fermi surface will be pushed through the Fermi surface, resulting in the possibility of one of the highly degenerate Landau levels coinciding with the Fermi level itself. This, in turn, will generate a significant enhancement of thermodynamic and electronic properties which depend on the density of states (DOS) at the Fermi level. Alternatively, one can think of all of the Landau levels which satisfy the quantization condition for motion perpendicular to the field axis as being arranged in a stack in k-space, known as a Landau tube. The length of the tube which falls between the intersection of its width with the constant energy surface for $\mathcal{E}$ and the surface for $\mathcal{E} + \Delta\mathcal{E}$ comprises the contribution to the density of states at $\mathcal{E}$. When the field strength is tuned such that the width of the Landau tube coincides with that of an extremal orbit on the Fermi surface, the length of the tube between $\mathcal{E}$ and $\mathcal{E} + \Delta\mathcal{E}$ is maximized. That is, having the field strength such that an extremal orbit on the Fermi surface satisfies the orbit quantization condition leads to a significant enhancement of the DOS, which diminishes once again as the field strength is fur-

ther increased, until yet another Landau level is encountered and the enhancement returns. This is the mechanism whereby oscillatory behaviour in the properties of the system which depend on the DOS at the Fermi level is produced.

From the foregoing discussion, there are two key ingredients for the observation of QO:

- A Fermi surface with *closed* cross-sectional areas, so that the orbit quantization condition can be satisfied for an extremal cross-section. A corollary of this stipulation is that the observation of QO is typically taken as evidence for a Fermi surface.

- Landau levels in the vicinity of the Fermi level, or, in the language to be used subsequently in this work, Landau levels in the low-energy DOS of the excitation spectrum.

The key utility of QO is that by using (1.1), an expression can be obtained which connects the extremal orbits of the Fermi surface, $A_e(\mathcal{E}_F)$, to the change in the reciprocal of the field strength on going from one oscillation to the next:

$$\Delta\left(\frac{1}{H}\right) = \frac{2\pi e}{\hbar c}\frac{1}{A_e(\mathcal{E}_F)}. \tag{1.2}$$

This property effectively enables one to "map" the Fermi surface by changing the orientation of the magnetic field and relating the change in the oscillations to the corresponding extremal cross-sectional areas. Given that the normal state properties of the underdoped cuprates are particularly anomalous, this ability to probe the Fermi surface structure – even, as it is, in the magnetic-field-induced normal state – provides invaluable insight into the electronic nature of these materials.

1.2.2 Experimental Observations of QO in the Cuprates.

The first observation of QO in the cuprates was in the electrical resistance of underdoped, oxygen-ordered $YBa_2Cu_3O_{6.5}$ (YBCO), where the oxygen atoms are in a well-ordered superstructure with minimal chemical disorder (Doiron-Leyraud et al., 2007). A low oscillation frequency was found, which is consistent with small Fermi surface pockets in the magnetic-field-induced normal state. Those authors attribute this to either: a part of the band structure specific to underdoped YBCO (the overdoped case has a large, open cylindrical Fermi surface); or to the formation of small pockets which occur as a result of a topological change at a critical point in the phase diagram (which would then be a more generic feature). Following these findings, LeBoeuf et al. (2007) observed a negative Hall resistance, implying that the observed Fermi surface pockets were associated with *electron* carriers, in spite of the fact that the material is *hole*-doped. This observation was proposed to be associated with Fermi surface reconstruction due to the onset of a density wave phase, since there is also evidence for such phases in the La_2CuO_4 family (Tranquada et al., 1995) and in $Bi_2Sr_2CaCu_2O_{8+x}$ (Parker et al., 2010). Subsequently, Sebastian et al. (2008) and Jaudet et al. (2008) observed the de Haas-van Alphen effect (oscillations in the magnetic susceptibility – a thermodynamic property) in YBCO, including a multi-component Fermi surface. Oscillations in the conductivity (the Shubnikov-de Haas effect) have also been observed (Bangura et al., 2008), which obtained Fermi surface pockets of a similar size to, and an effective charge carrier mass consistent with, the original observations in Doiron-Leyraud et al. (2007). Additional studies have since demonstrated that these oscillations and the associated Fermi surface pockets are a generic feature of the cuprates (Rourke et al., 2010; Singleton et al., 2010; Yelland et al., 2008).

A more recent study of QO in the heat capacity of YBCO right through the magnetic-field-induced resistive transition has added an additional dimension to the already established QO phenomena. Riggs et al. (2011) attempted to resolve the question of whether the application of the field destroys the d-wave gap and reveals a Fermi-liquid-like normal state, or whether the field merely eliminates the long-range phase coherence of the superconductivity, while the gap itself persists. What was found was that, at very high fields, the specific heat exhibits conventional temperature-dependence and QO consistent with a Fermi liquid. However, the observed field-dependence of the quasiparticle DOS in a field of strength H goes like $\sqrt{H}$, and is unaffected by the resistive transition. This behaviour suggests an entrenched d-wave gap over the entire field range measured. At low H, and below the lower critical field, this is consistent with the nodes of the d-wave gap dominating the thermodynamic properties, but the persistence into the resistive state instead implies a strong correlation picture, which is necessary to maintain the gap in spite of the absence of long-range superconductivity (Tesanovic, 2011). Furthermore, Riggs et al. (2011) find that the absolute value of the specific heat is too small to be adequately compatible with the simple Fermi surface reconstruction scheme which emerges from the interpretation of the results in (Doiron-Leyraud et al., 2007), *etc.*, as Fermi surface pockets. This opens the door to alternative explanations concerning the origin of the oscillatory phenomena.

1.3 The π-Striped Superconductor and Quantum Oscillations

Several proposals exist which are designed to explain the phenomena discussed in Section 1.2. The most straightforward has been eluded to in conjunction with the results in Doiron-Leyraud et al. (2007), and consists of Fermi surface reconstruction

via a density wave. For example, Harrison (2009) and Millis and Norman (2007) have suggested that Fermi surface reconstruction by various types of spin-density waves (SDW) could also reorganize the large hole Fermi surface of the undistorted lattice into the necessary pockets, and is possibly consistent with the multiple observed QO frequencies in Sebastian et al. (2008). Similarly, a weak, unidirectional charge density wave (CDW) with a periodicity of four lattice constants (consistent with observations of such a state in NMR experiments on YBCO) can reconstruct the Fermi surface of a typical hole-doped cuprate to produce and electron pocket of roughly the requisite size and effective mass (Yao et al., 2011). It has also been suggested that correlation effects – such as orbital-dependent band distortions and anisotropic self-energy corrections – must be incorporated into Fermi surface reconstruction approaches (Elfimov et al., 2008). However, as mentioned above, these approaches encounter difficulties with both the observation by Riggs et al. (2011) of the persistent $\sqrt{H}$ background in the specific heat found and the relatively small specific heat magnitude. Alternatively, there have been proposals that the QO emerge from the quantum interference of the vortex lattice and the lattice modulations of the order parameter (Alexandrov, 2008), or that dispense with reconstruction altogether and develop a mechanism for obtaining QO directly from the Fermi arcs observed by ARPES (Pereg-Barnea et al., 2010).

On the other hand, recent work on an antiphase *pair* density wave (PDW) – a sinusoidal modulation of the SC gap function over a period of eight lattice constants – has demonstrated a means of obtaining both a reconstructed Fermi surface with pockets of the appropriate size, as well as a persistent SC gap amplitude (Zelli et al., 2011, 2012). It has been shown to be possible in strongly correlated, $2D$ electronic systems to construct a state where the SC condensate has nonzero wavevector and double the spatial period of the attendant CDW (Berg et al., 2007). This particular

type of PDW goes by the moniker of the π-striped superconductor.[1] The general PDW order parameter is designed to vary periodically as a function of position, such that when averaged over the centre-of-mass position, it vanishes identically (Berg et al., 2009). It was originally proposed as a means of explaining the dynamical decoupling of layers in transport measurements at 1/8 doping in LBCO, since it produces identically zero Josephson coupling between the layers (Berg et al., 2007; Himeda et al., 2002). It has also been invoked to explain scanning tunneling microscopy (STM) measurements which demonstrate weak translational symmetry breaking, on the grounds that a CDW alone is insufficient to explain these measurements, but that modulation of the hopping or pairing can (Podolsky et al., 2003). Variational Monte Carlo (VMC) and renormalized mean-field theory (RMFT) calculations have demonstrated that the π-striped SC has a free energy which is quite close to that of the uniform SC case (Raczkowski et al., 2007).

In terms of its relevance to QO experiments, the antiphase modulated d-wave SC exhibits an extended Fermi surface with many small pockets (the size of which is dependent on the gap amplitude), in contrast to the uniform d-wave case where the Fermi surface consists of the four nodal points (Zelli et al., 2011). Those authors were also able to study the mixed state using Bogoliubov-de Gennes (BdG) theory (de Gennes, 1966), and found the other necessary ingredient for QO: Landau levels in the low energy DOS, which in this case are a coherent mixture of particles and holes. However, the field strengths in this study were constrained by the requirement of the magnetic unit cell being commensurate with the period of the SC modulation, and the gap amplitude was taken as an input parameter. Additional work, using a semiclassical approach to neglect the vortex structure, which enabled smoother vari-

[1] With the "π" denoting the sign change in the gap between adjacent CDW domains which comprise the period of the SC modulation.

ation of the magnetic field, was able to connect closed pieces of the extended Fermi surface with the experimental observations of QO in the cuprates (Zelli et al., 2012). The logical extension of these works is to use the full machinery of the self-consistent BdG method to attempt to stabilize the π-striped state at a mean-field level from a microscopic Hamiltonian which is representative of cuprate physics. Ultimately, the goal would be to study the self-consistent equations in a magnetic field without assuming a fixed, two-dimensional array of vortices or making use of the semiclassical approximation employed by Zelli et al. (2012). However, a first step is to study the self-consistent solutions in zero field. This constitutes the objective of the present work.

Chapter 2

The π-Striped Superconductor and a Charge-Density Wave Phase

One of the key aspects of the π-striped modulation of the superconductivity is that it is commensurate with the CDW modulation of the charge (Berg et al., 2007). In fact, this intertwining modulation of the charge- and pair-densities is one of the crucial aspects necessary to explain certain experimental results (Podolsky et al., 2003). In previous studies of the π-striped SC, where this form of order is proposed as an alternative to the Fermi surface reconstruction by CDW/SDW explanation of QO in the cuprates, the focus has been on the PDW aspect of the model. In this chapter, the CDW itself is incorporated into the model, to determine what the qualitative impacts are on the results of Zelli et al. (2011) on the mixed state of the π-striped SC. This chapter provides theoretical details of the π-striped SC, followed by an exposition of its electronic properties – with and without an external magnetic field, and with and without accompanying CDW order.

2.1 A Model for the π-Striped Superconductor

The π-striped SC describes a condensate with nonzero wavevector and no net gap amplitude when averaged over the period of the modulation (Berg et al., 2007, 2009).

It has been studied in non-self-consistent Bogoliubov-de Gennes theory, using a mean-field effective Hamiltonian (Baruch and Orgad, 2008; Zelli et al., 2011):

$$\begin{aligned} H_{\text{eff}} \quad = \quad & -\sum_{i\delta\sigma} t c^{\dagger}_{i\sigma} c_{i+\delta,\sigma} - \sum_{i\sigma} \mu c^{\dagger}_{i\sigma} c_{i\sigma} \\ & + \sum_{xy} \Delta \Big\{ \cos\left(Q_x x\right) \left[c^{\dagger}_{x,y,\uparrow} c^{\dagger}_{x+1,y,\downarrow} + c^{\dagger}_{x+1,y,\uparrow} c^{\dagger}_{x,y,\downarrow} \right] \\ & - \cos\left[Q_x (x-1/2)\right] \left[c^{\dagger}_{x,y,\uparrow} c^{\dagger}_{x,y+1,\downarrow} + c^{\dagger}_{x,y+1,\uparrow} c^{\dagger}_{x,y,\downarrow} \right] + \text{H.C.} \Big\}, \end{aligned} \tag{2.1}$$

where μ is the chemical potential, Δ is the magnitude of the SC gap, and t is the nearest-neighbour hopping energy (which sets the energy scale for the problem), with δ representing hopping in $\pm\hat{\mathbf{x}}$ and $\pm\hat{\mathbf{y}}$ direction. The operator $c^{\dagger}_{i\sigma}$ ($c_{i\sigma}$) creates (annihilates) an electron with spin σ on site i, whose position is given by $\mathbf{r}_i = x\hat{x} + y\hat{y}$ (with $\hat{x}$ and $\hat{y}$ being unit vectors in the given directions). Note that the form of the Hamiltonian ensures that all pairing occurs into singlet states. The modulation described by the cosine factors in equation (2.1) reflects a bond-centred geometry on a square lattice, wherein a given pair creation $c^{\dagger}_{x,y,\uparrow} c^{\dagger}_{x+1,y,\downarrow}$ along the x-direction (for example) takes place on the bond between the site with index x and that with index $x+1$. The offset of half of a lattice constant in the y-direction modulation reflects the fact that y-direction bonds are located directly at the x coordinate of a given site. Finally, the modulation wavevector Q_x in this case has the value of $\pi/4$, which introduces a periodicity of 8 sites. This is in order to be consistent with the considerations in Berg et al. (2007), which necessitate that the period of the SC modulation be twice that of the CDW.[1] As a result of the 8 site periodicity, the wavevector of each electron in k-space is only coupled to seven other wavevectors (Zhou et al., 2011), which results in a reduced Brillouin zone (RBZ) with the eight pieces of the extended zone scheme

[1] The period of the CDW has been established as four sites in the cuprates which are known to harbour charge order (Yao et al., 2011).

folded back into it.

Note that other PDW configurations exist which are consistent with period-4 CDWs. Baruch and Orgad (2008) also describe an "in-phase" PDW, in which the modulation does not change sign as it crosses adjacent charge domains, as well as a site-centred version of the π-striped PDW given by (2.1). They find that the in-phase PDW exhibits the same low-energy excitation spectrum as the uniform case, consisting solely of the four nodal points. On the other hand, the site-centred antiphase PDW has been found to have the same qualitative features as the bond-centred π-striped version (Baruch and Orgad, 2008; Zelli et al., 2011).

2.2 The Bogoliubov-de Gennes Method

In order to describe an inhomogeneous SC state, or one which experiences an external potential, it is necessary to use the Bogoliubov-de Gennes (BdG) method, which is essentially a generalization of the Hartree-Fock method for the interacting electron gas (de Gennes, 1966). The unitary BdG transformation is given by

$$c_{i\sigma} \equiv \sum_n \left[u_i^n \gamma_{n\sigma} - \sigma v_i^{n*} \gamma_{n,-\sigma}^\dagger \right]. \tag{2.2}$$

In this transformation, the electron operators are separated into a superposition of quasiparticle operators – the $\gamma_{n\sigma}$ – which effectively combine the electron with its time-reversed partner, *i.e.* a hole.[2] The (u_i^n, v_i^n) are the components of the BdG wavefunction, with n as a state index. The quasiparticle operators $\gamma_{n\sigma}$ are assumed

[2] As can be observed by inverting the transformation.

to have the following mean-value rules (de Gennes, 1966):

$$\begin{aligned} \langle \gamma^{\dagger}_{n\sigma} \gamma^{\dagger}_{n'\sigma'} \rangle &= \langle \gamma_{n\sigma} \gamma_{n'\sigma'} \rangle = 0 \\ \langle \gamma^{\dagger}_{n\sigma} \gamma_{n'\sigma'} \rangle &= 1 - \langle \gamma_{n\sigma} \gamma^{\dagger}_{n'\sigma'} \rangle = f_{n\sigma} \delta_{n'n} \delta_{\sigma'\sigma}, \end{aligned} \tag{2.3}$$

where $f_{n\sigma}$ is the occupation function for quasiparticles in state n with spin σ, and is the standard fermionic occupation function. They are also assumed to obey fermionic anti-commutation relations:

$$\{\gamma_{n\sigma}, \gamma^{\dagger}_{n'\sigma'}\} = \delta_{n'n} \delta_{\sigma'\sigma}. \tag{2.4}$$

It can be shown that in the quasiparticle representation, the effective Hamiltonian in (2.1) will become diagonal; that is,

$$H_{\text{eff}} = \sum_{n\sigma} E_n \gamma^{\dagger}_{n\sigma} \gamma_{n\sigma} + E_0, \tag{2.5}$$

where E_0 is the ground-state energy, and E_n defines the dispersion of excitations out of the ground state.

The BdG equations express the quasiparticle dispersion of the system in terms of the BdG wavefunction embodied in the (u^n_i, v^n_i), and form the connection with the original effective Hamiltonian which must be satisfied in order for the diagonalization to hold. The traditional route to the BdG equations is through the commutator $[c_{i\sigma}, H_{\text{eff}}]$, with H_{eff} given both by (2.1) and by its diagonal form in the quasiparticle basis, equation (2.5), with the electron operators expressed in terms of the quasiparticle operators. The derivation is carried out in Appendix A for the case of uniform

SC, but the final result carries over directly to the π-striped case, and is given by

$$\begin{aligned} E_n u_i^n &= -\sum_\delta t u_{i+\delta}^n - \mu u_i^n \\ &+ \Delta\cos(Q_x x) v_{x+1,y}^n + \Delta\cos[Q_x(x-1)] v_{x-1,y}^n \\ &- \Delta\cos[Q_x(x-1/2)][v_{x,y+1}^n + v_{x,y-1}^n] \\ E_n v_i^n &= \sum_\delta t v_{i+\delta}^n + \mu v_i^n \\ &+ \Delta^*\cos(Q_x x) u_{x+1,y}^n + \Delta^*\cos[Q_x(x-1)] u_{x-1,y}^n \\ &- \Delta\cos[Q_x(x-1/2)][u_{x,y+1}^n + u_{x,y-1}^n]. \end{aligned} \tag{2.6}$$

These equations are conveniently expressed in the following matrix form:

$$\begin{bmatrix} \hat{\xi} & \hat{\Delta} \\ \hat{\Delta}^* & -\hat{\xi}^* \end{bmatrix} \begin{pmatrix} u_i^n \\ v_i^n \end{pmatrix} = E_n \begin{pmatrix} u_i^n \\ v_i^n \end{pmatrix}, \tag{2.7}$$

with

$$\hat{\xi} u_i^n \equiv -\sum_\delta t u_{i+\delta}^n - \mu u_i^n \tag{2.8}$$

$$\begin{aligned} \hat{\Delta} v_i^n &\equiv \Delta\cos(Q_x x) v_{x+1,y}^n + \Delta\cos[Q_x(x-1)] v_{x-1,y}^n \\ &- \Delta\cos[Q_x(x-1/2)][v_{x,y+1}^n + v_{x,y-1}^n]. \end{aligned} \tag{2.9}$$

2.3 Block-Diagonalization of the BdG Equations

The condensed matter physicist frequently encounters periodic arrays (*e.g.* of ions), and thus finds frequent use for discrete translational symmetry in defining or simplifying a problem. The most common implication of discrete translational symmetry is the standard Bloch theorem, which states that eigenstates $\psi(\mathbf{r})$ of a Hamiltonian H with a periodic potential can be chosen such that $\psi_{\mathbf{k}}(\mathbf{r}+\mathbf{R}) = e^{i\mathbf{k}\cdot\mathbf{R}}\psi_{\mathbf{k}}(\mathbf{r})$, for every

R in the Bravais lattice, which encapsulates the notion that the discrete translation operator and the Hamiltonian must commute (Ashcroft and Mermin, 1976). However, when the discrete translational symmetry of the Bravais lattice is further broken by some superlattice potential, it is necessary to apply the Bloch theorem up to a unit cell translation vector which instead reflects the periodicity of the superlattice. In the present work, this formalism is adopted in order to handle the modulation of the SC order, which breaks the translational symmetry of the lattice with a unit cell reflecting the translational symmetry of the period-8 modulation of the SC order. While there is no constraint on the number of sites along the y-direction, N_y, because the PDW is unidirectional, it is necessary to have $N_x = 8N_x'$, where $N_x' \in \mathbb{N}$ is the number of modulation periods within the unit cell.

To implement the Bloch theorem up to the translational symmetry of the π-striped SC, the site indices are redefined as $i = (x, y) \longrightarrow i = (x + R_x, y + R_y)$, where $\mathbf{R} = R_x\hat{x} + R_y\hat{y}$ is the translation vector for the modulation unit cell, and i is now understood to range only over the sites contained in a given reference unit cell. The components of the BdG wavefunction (u_{xy}^n, v_{xy}^n) undergo the following transformation:

$$u_{xy}^n(\mathbf{R}) = \frac{1}{N_{k_x}} \sum_{\mathbf{k}} e^{i(k_x R_x + k_y R_y)} u_{xy}^n(\mathbf{k}) \tag{2.10}$$

$$v_{xy}^n(\mathbf{R}) = \frac{1}{N_{k_y}} \sum_{\mathbf{k}} e^{i(k_x R_x + k_y R_y)} v_{xy}^n(\mathbf{k}), \tag{2.11}$$

where $k_x = 2\pi m_x / 8N_{k_x}N_x'$ and $k_y = 2\pi m_y / N_{k_y}N_y$, with $m_x = 0, 1, ..., N_{k_x} - 1$ and $m_y = 0, 1, ..., N_{k_y} - 1$. Similarly, $R_x = 8\alpha_x N_x'$ and $R_y = \alpha_y N_y$, where $\alpha_x, \alpha_y \in \mathbb{Z}$.

Additionally, as a consequence of the particle-hole symmetry of the BdG equations, there is a symmetry between E_n and $-E_n$ (de Gennes, 1966), which yields the

following correspondence in the BdG wavefunction components for $\mathbf{k}$ and $-\mathbf{k}$:

$$\begin{pmatrix} u_{xy}^{n}(\mathbf{k}) \\ v_{xy}^{n}(\mathbf{k}) \end{pmatrix} \longrightarrow \begin{pmatrix} -v_{xy}^{n*}(-\mathbf{k}) \\ u_{xy}^{n*}(-\mathbf{k}) \end{pmatrix}. \tag{2.12}$$

This property enables the execution time of the BdG code to be halved, since the eigenvalues and eigenvectors for $-\mathbf{k}$ can be determined from those for $+\mathbf{k}$.

2.4 BdG Calculations for a π-Striped Superconductor

Under the unit cell transformation discussed in Section 2.3, the BdG equations for the π-striped SC in equation (2.7) now take on the following form in the bulk for a given $\mathbf{k}$:

$$\begin{bmatrix} \hat{\xi}(\mathbf{k}) & \hat{\Delta}(\mathbf{k}) \\ \hat{\Delta}^{*}(\mathbf{k}) & -\hat{\xi}^{*}(\mathbf{k}) \end{bmatrix} \begin{pmatrix} u_{i}^{n}(\mathbf{k}) \\ v_{i}^{n}(\mathbf{k}) \end{pmatrix} = E_{n} \begin{pmatrix} u_{i}^{n}(\mathbf{k}) \\ v_{i}^{n}(\mathbf{k}) \end{pmatrix}, \tag{2.13}$$

with

$$\hat{\xi}(\mathbf{k})u_{i}^{n}(\mathbf{k}) \equiv -\sum_{\delta} t u_{i+\delta}^{n}(\mathbf{k}) - \mu u_{i}^{n}(\mathbf{k}) \tag{2.14}$$

$$\begin{aligned} \hat{\Delta}v_{i}^{n}(\mathbf{k}) \equiv\ & \Delta\cos\left(Q_{x}x\right)v_{x+1,y}^{n}(\mathbf{k}) + \Delta\cos\left[Q_{x}(x-1)\right]v_{x-1,y}^{n}(\mathbf{k}) \\ & -\ \Delta\cos\left[Q_{x}(x-1/2)\right][v_{x,y+1}^{n}(\mathbf{k}) + v_{x,y-1}^{n}(\mathbf{k})]. \end{aligned} \tag{2.15}$$

By numerically diagonalizing (2.13), one obtains the eigenvectors which contain the BdG wavefunction. These can then be utilized to calculate the local density of states (LDOS), $\rho(i,E)$, which is the DOS at each site i in the unit cell at a particular energy level E. In terms of the $(u_{i}^{n}(\mathbf{k}), v_{i}^{n}(\mathbf{k}))$, the LDOS has the following form (Zelli

et al., 2011):

$$\rho(i,E) = 2\sum_{n\mathbf{k}} \left[|u_i^n(\mathbf{k})|^2\delta(E-E_n) + |v_i^n(\mathbf{k})|^2\delta(E+E_n)\right], \tag{2.16}$$

where the summation is restricted to positive-energy eigenvectors.[3] The DOS itself is then obtained by summing over the position index in (2.16). A related quantity is the spectral function $A(\mathbf{q},E)$, which can be viewed as the LDOS in reciprocal space, providing the density of states at each $\mathbf{q}$ value for a particular energy. It is important to note the distinction between the Bloch $\mathbf{k}$ values, which reflect the superlattice translational symmetry, and the $\mathbf{q}$ values being introduced here; the latter are the result of Fourier transformation of the BdG wavefunction *within* the unit cell. That is,

$$A(\mathbf{q},E) = \frac{2}{N_s N_{\mathbf{k}}}\sum_{n\mathbf{k}} \left[|u_{\mathbf{q}}^n(\mathbf{k})|^2\delta(E-E_n) + |v_{\mathbf{q}}^n(\mathbf{k})|^2\delta(E+E_n)\right], \tag{2.17}$$

where N_s is the number of sites in the unit cell, and $(u_{\mathbf{q}}^n(\mathbf{k}), v_{\mathbf{q}}^n(\mathbf{k}))$ is the Fourier-transformed BdG wavefunction (Zelli et al., 2011). The analogy with the LDOS is immediately clear from the form of (2.17). In addition, the Fermi surface can be readily obtained from the spectral function by taking a cut at $E = 0$, and "unfolding" the result in order to tile the extended Brillouin zone (since $A(\mathbf{q},E)$ is defined within the reduced Brillouin zone, which condenses the eight-fold translational symmetry of the extended Brillouin zone that is introduced by the period-8 modulation). Thus, between them, $\rho(i,E)$ and $A(\mathbf{q},E)$ provide considerable insight into the electronic properties of a system.

[3] The factor of two denotes the spin-symmetry in the present case.

2.5 Competition with a Charge-Density Wave

The CDW can now be introduced into the model of the π-striped SC given by the effective Hamiltonian (2.1). It can be represented by the addition of the following term (Baruch and Orgad, 2008):

$$H_{\mathrm{CDW}} = \sum_{xy\sigma} V_c \cos[2Q_x(x+1/2)] c^{\dagger}_{x,y,\sigma} c_{x,y,\sigma}, \tag{2.18}$$

where V_c is the energy scale associated with the CDW. The doubling of the ordering wavevector Q_x in the modulation reflects the fact that the periodicity of the CDW is half of that of the π-striped modulation. The half-lattice-constant offset is intended to ensure that the charge excesses produced by the CDW coincide with the sites where the PDW amplitude is at a maximum, and vice versa. In all cases, the chemical potential μ is adjusted to yield 1/8 doping, which is the canonical doping level for the π-striped model, and the spectral width about zero energy is $-0.02t < E < 0.02t$. Additionally, all the results are given for $\Delta = 0.25t$, which corresponds to the so-called "intermediate regime" Zelli et al. (2011). The calculations in this section are based on computer code by Saaed Zelli which implemented non-self-consistent BdG for the π-striped SC, and which was modified in the present work to include the CDW order.

In this regime in the absence of the CDW, the closed loops in the Fermi surface which exist at small Δ have been gapped out, and the spectral function exhibits Fermi arcs with two small intervening gaps (see Figure 2.1). Increasing the CDW amplitude to $V_c = 0.30t$ in Figure 2.2 introduces fairly minimal changes in the Fermi surface structure. There is a slight increase in the separation of the FS pockets with increasing V_c, compared with their practically conjoined appearance in Figure 2.1. However, the

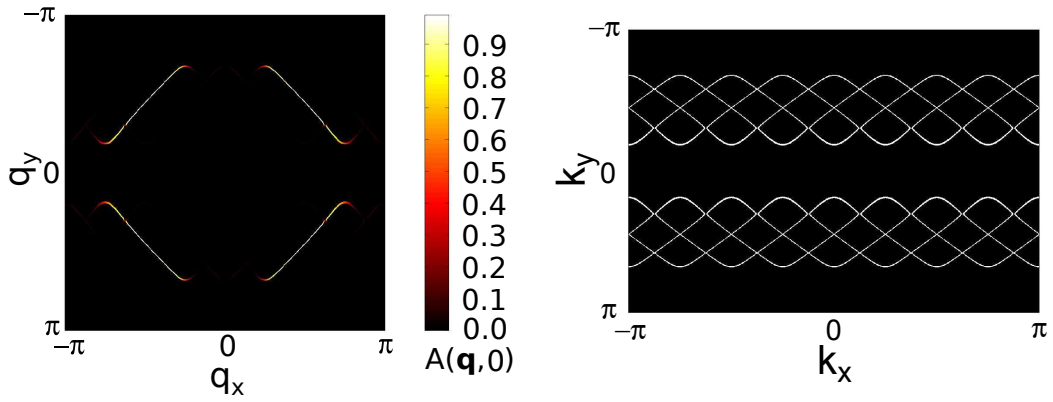

(a) Spectral Function (b) Fermi Surface

Figure 2.1: $\Delta = 0.25t$, $V_c = 0.00t$ and $\mu = -0.32t$ ($\approx 7/8$ filling). $N_x = N_y = 8$, with $N_{k_x} = N_{k_y} = 96$. The spectral width is $-0.02t < E < 0.02t$.

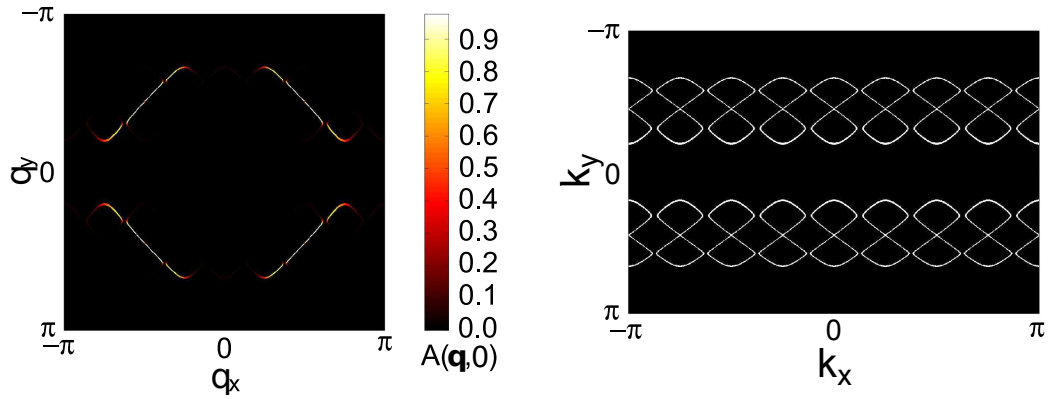

(a) Spectral Function (b) Fermi Surface

Figure 2.2: $\Delta = 0.25t$, $V_c = 0.30t$ and $\mu = -0.32t$. $N_x = N_y = 8$ with $N_{k_x} = N_{k_y} = 96$. The spectral width is $-0.02t < E < 0.02t$.

effect of the CDW is much more pronounced on the Landau level structure, as will be demonstrated in the following section.

2.5.1 Charge Density Wave in Magnetic Field

The foregoing analysis is now extended to include a magnetic field and generate Landau levels. The theoretical details on how this is implemented for the π-striped SC can be found in Zelli et al. (2011). Following the convention in that study, the field strength B is defined by the flux quantum $\phi_0 = Bl^2$, so that it is expressed in terms of the size, l, of the magnetic unit cell which contains two vortices. The vector potential breaks the translational symmetry of the lattice, however it is possible to define new magnetic translation operators which do commute with the Hamiltonian (Brown, 1964; Zak, 1964a,b), and thereby block-diagonalize it just as with the superlattice potential discussed in Section 2.3. Further, the vector potential is expressed in the Franz-Tesanovic gauge, which is a special case where the magnetic translation operators coincide with the superlattice translation operators. The block-diagonalization into magnetic unit cells also acts as a significant efficiency boost for limited computational resources. If there are N_{k_x} magnetic unit cells along the x-direction and N_{k_y} along the y-direction, with $N_x \times N_y$ sites comprising a magnetic unit cell, then a system of $N_{k_x}N_x \times N_{k_y}N_y$ sites block-diagonalizes into $N_{k_x} \times N_{k_y}$ separate eigenvalue problems, each with $N_x \times N_y$ sites involved in the matrix. Because computational time for numerical diagonalization scales with the third power of the linear size of the matrix, this constitutes a considerable savings of computational resources.

The negative- and positive-energy DOS distributions for $V_c = 0.00t$ and $l = 24$ are plotted in Figure 2.3. This plot essentially reproduces an equivalent figure in Zelli et al. (2011), demonstrating agreement between the core results of that study and the present work. Figure 2.4 gives the same calculation, but repeated for a CDW gap of

$V_c = 0.30t$. With this magnitude of V_c, the figure demonstrates that the robustness of the Landau levels is greatly diminished. A larger unit cell (and hence, a weaker field) is then utilized in Figures 2.5 and 2.6 in order to examine the effect of field strength on the DOS and the Landau level formation. For both this field strengths and that used in the previous figures, when V_c is large there is an apparent "washing out" of the Landau level structure.

To be semi-quantitative about the Landau level collapse with increasing V_c (*i.e.* a decay in the periodicity of the Landau levels), a harmonic analysis of the DOS was conducted in the low energy region of $-\Delta < E < +\Delta$.[4] The Fourier weight obtained from this transform was converted into the standard power spectrum given by

$$P(\omega) = \sqrt{|\mathcal{F}(\mathrm{DOS}(E))|^2}, \tag{2.19}$$

where P is the intensity at a particular frequency ω and $\mathcal{F}(\mathrm{DOS}(E))$ is the Fourier-transform of the DOS from the E domain to the ω domain. In Figure 2.7, the power spectra for $V_c = 0.00t_1$ and $V_c = 0.30t_1$ at a field strength corresponding to $l = 24$ are compared (similarly for the $l = 32$ case with Figure 2.8); the positions of the non-trivial frequency weight[5] are noted and the intensity, P at those points is plotted as a function of several V_c in Figure 2.9a (Figure 2.9b for $l = 32$). This provides a semi-quantitative indication of the Landau level collapse with increasing V_c, wherein the frequency weights function as a sort of order parameter for the Landau levels. If the frequency weight is decreasing for a particular oscillation channel in the DOS spectrum, then the phenomenon which generates that oscillation is decreasing in strength relative to the background. Clearly then, for a sufficiently strong CDW component in competition with the PDW, there would be no observation of QO, since

[4] The "sawtooth" region with well-resolved Landau levels in the low-energy DOS; see Figure 2.3.

[5] Aside from the zero-frequency spike in the centre.

the Landau levels which lead to the QO have become too degraded. The qualitative observation of the Landau level degradation is also the same for both of the field strengths examined, with the exception that the field corresponding to $l = 24$ has multiple Landau level spacings.[6] As discussed in Zelli et al. (2011), the Landau levels are a result of magnetic breakdown, whereby quasiparticles tunnel between orbits on closely separated pockets of the Fermi surface. As can be observed by contrasting Figures 2.2b and 2.1b, the effect of the CDW is to modestly increase the gap in k-space between these pockets, with the result that the probability of the quasiparticle tunneling between the orbits contained on the separate pockets becomes greatly diminished. Zelli et al. (2011) found a similar effect for large Δ, which also produces isolated Fermi surface pockets, as opposed to the small-to-intermediate Δ regime.

[6]The reason for this is discussed in Zelli et al. (2011), and essentially has to do with whether there are an odd or even number of SC modulation periods in the reference unit cell.

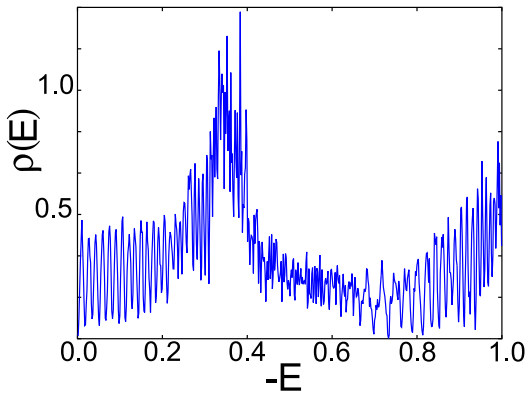

(a) $E < 0$

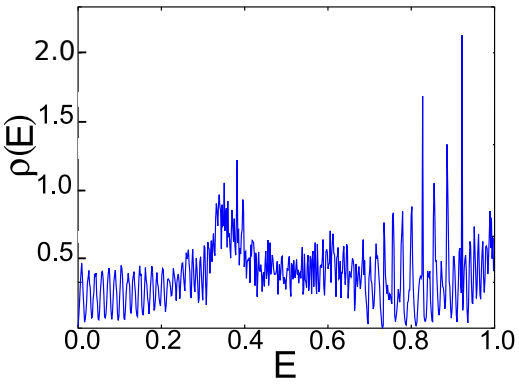

(b) $E > 0$

Figure 2.3: DOS for $\Delta = 0.25t$, $V_c = 0.00t$ and $\mu = -0.32t$ with $l = 24$ and $N_{k_x} = N_{k_y} = 96$. The energy width for the binning of the DOS is 4×10^{-5}.

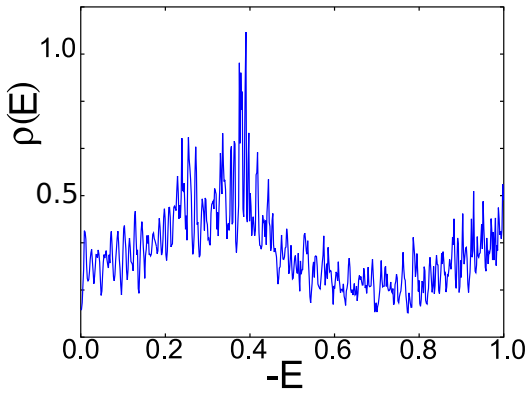

(a) $E < 0$

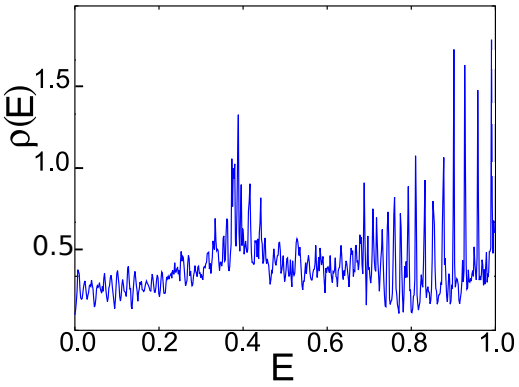

(b) $E > 0$

Figure 2.4: DOS for $\Delta = 0.25t$, $V_c = 0.30t$ and $\mu = -0.32t$ with $l = 24$ and $N_{k_x} = N_{k_y} = 96$. The energy width for the binning of the DOS is 4×10^{-5}.

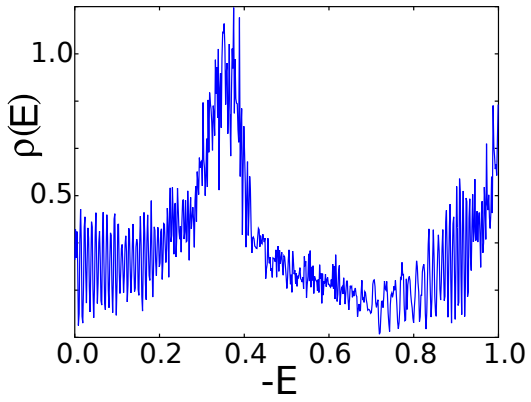

(a) $E < 0$

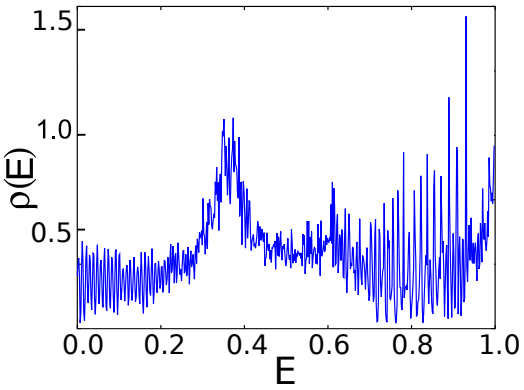

(b) $E > 0$

Figure 2.5: DOS for $\Delta = 0.25t$, $V_c = 0.00t$ and $\mu = -0.32t$ with $l = 32$ and $N_{k_x} = N_{k_y} = 96$. The energy width for the binning of the DOS is 4×10^{-5}.

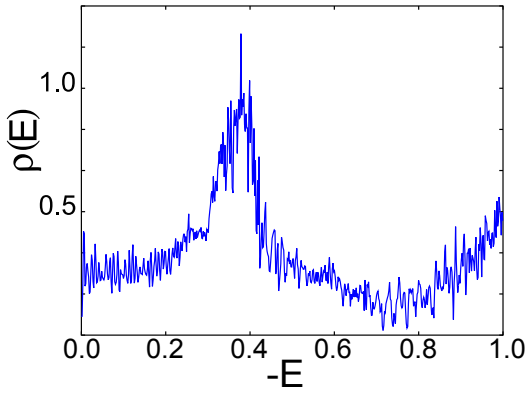

(a) $E < 0$

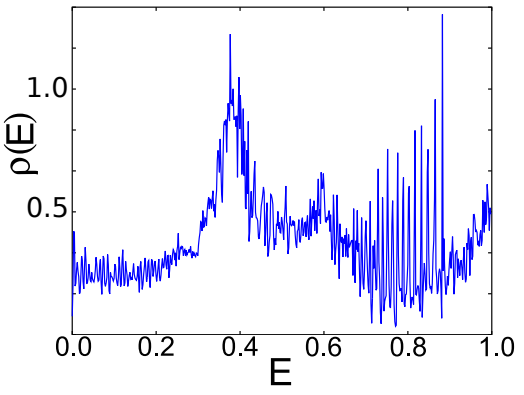

(b) $E > 0$

Figure 2.6: DOS for $\Delta = 0.25t$, $V_c = 0.30t$ and $\mu = -0.32t$ with $l = 32$ and $N_{k_x} = N_{k_y} = 96$. The energy width for the binning of the DOS is 4×10^{-5}.

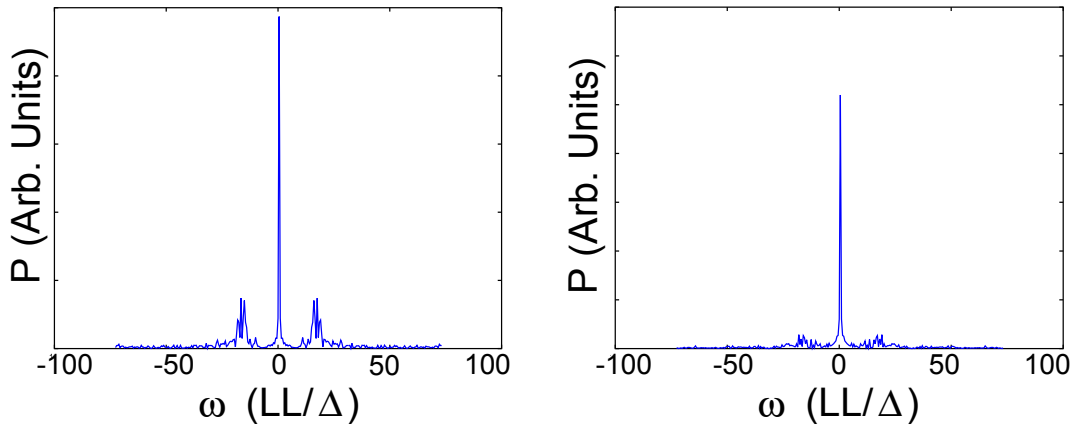

(a) $\Delta = 0.25t$ and $V_c = 0.00t$ (b) $\Delta = 0.25t$ and $V_c = 0.30t$

Figure 2.7: Landau level power spectra given by equation (2.19) comparing the null case with the case where the CDW magnitude is finite for a field strength corresponding to $l = 24$. The transformed region is $-\Delta < E < +\Delta$. In both cases, $\mu = -0.32t$ and $N_{k_x} = N_{k_y} = 96$. The key frequency peaks used subesquently in Figure 2.9a correspond to 16 LL/Δ and 17.5 LL/Δ.

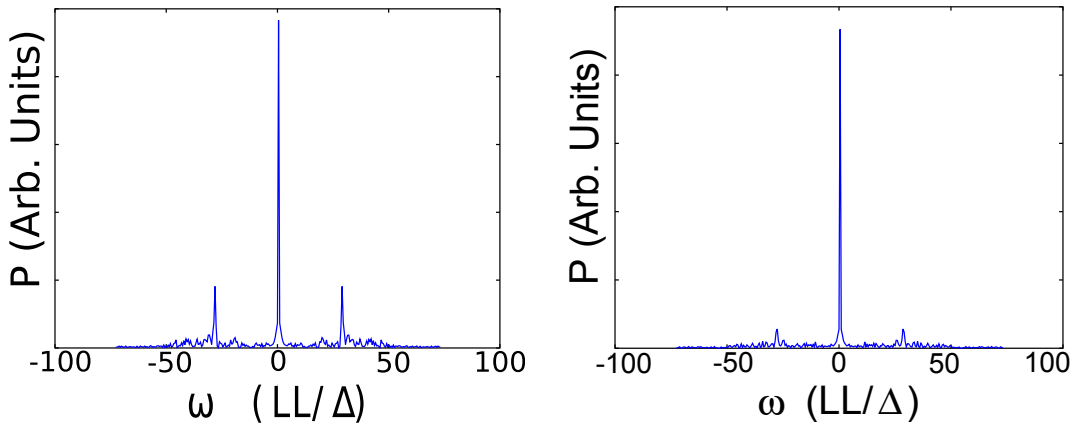

(a) $\Delta = 0.25t$ and $V_c = 0.00t$ (b) $\Delta = 0.25t$ and $V_c = 0.30t$

Figure 2.8: Landau level power spectra given by equation (2.19) comparing the null case with the case where the CDW magnitude is finite for a field strength corresponding to $l = 32$, weaker than the case exhibited in Figure 2.7. The transformed region is $-\Delta < E < +\Delta$. In both cases, $\mu = -0.32t$ and $N_{k_x} = N_{k_y} = 96$. The key frequency peak used subesquently in Figure 2.9b corresponds to 29 LL/Δ.

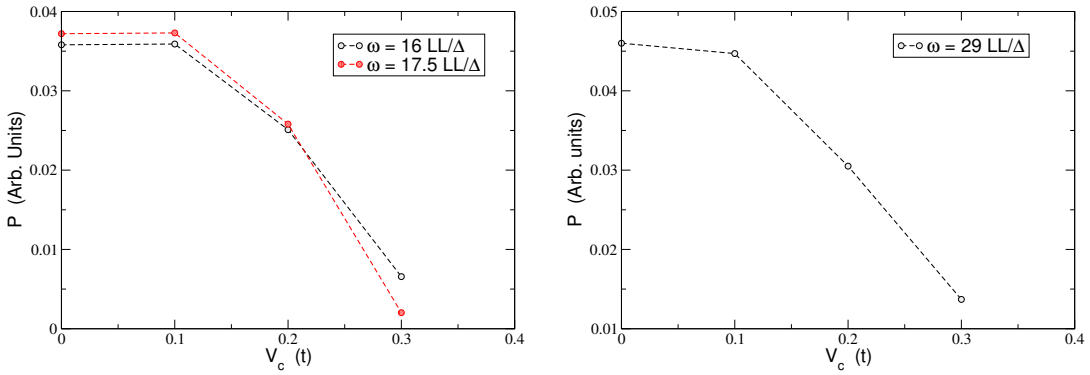

(a) $\Delta = 0.25t$ and $l = 24$ (b) $\Delta = 0.25t$ and $l = 32$

Figure 2.9: Frequency weights identified in Figures 2.7 and 2.8 as a function of V_c indicating the Landau level collapse with increasing V_c for the prominent peaks in the $V_c = 0.00t$ case.

Chapter 3

A Self-Consistent Approach to the π-Striped Superconductor

The model of the π-striped SC introduced in Chapter 2 is defined by a phenomenological, "mean-field" Hamiltonian. In mean-field models, the electron interactions are dealt with in an average sense (hence the name), which drastically simplifies the problem by recasting it in terms of a quadratic Hamiltonian, and thereby enables calculations to become tractable. A particular mean-field decomposition of a microscopic Hamiltonian is made self-consistent by determining the configuration of the mean-fields which minimize the variational free energy: the free energy of the microscopic Hamiltonian with respect to the eigenstates of the mean-field, effective Hamiltonian (de Gennes, 1966). This is termed "self-consistency" because the mean-fields depend on the effective Hamiltonian, which, in turn, depends on the values of the mean-fields. In the following sections, the π-striped mean-field Hamiltonian is connected with the t-J model, a microscopic model of cuprate superconductivity, which is considered to be the "minimal model" for this phenomenon (Norman and Pépin, 2003). The resulting self-consistent equations are then used to assess the stability of the π-striped SC at the mean-field level for a range of parameters. It was found that the π-striped state was not stable over the parameter range studied for

the mean-field t-J model, indicating that it has a higher free energy than the normal state. The free energy of the π-striped state was calculated with Δ treated in a parametric fashion away from the normal state, with several modifications to the Hamiltonian, in order to assess what factors might contribute to the stability of the π-striped state in treatments with extensions beyond the mean-field level.

3.1 The t-J Model

It has long been proposed (Anderson, 1987) that the physics of the CuO_2 planes which form the key structure of the cuprate SC is essentially encapsulated in the Hubbard model. The microscopic Hamiltonian for this model is given by (Hubbard, 1963):

$$H = -t \sum_{i\delta\sigma} c^{\dagger}_{i\sigma} c_{i+\delta,\sigma} - \mu \sum_{i\sigma} n_i + U \sum_{i} n_{i\uparrow} n_{i\downarrow}, \tag{3.1}$$

with

$$n_i = n_{i\uparrow} + n_{i\downarrow} = c^{\dagger}_{i\uparrow} c_{i\uparrow} + c^{\dagger}_{i\downarrow} c_{i\downarrow}. \tag{3.2}$$

In equation (3.1), the parameters t and μ, and the electron operators $c_{i\sigma}$, have the same definitions as stated for equation (2.1) in Chapter 2. The main feature of equation (3.1) is the on-site Coulombic repulsion term, whose energy scale is set by the parameter U (with $U > 0$ implying repulsion). As it was for the π-striped mean-field Hamiltonian, t is taken as the unit of energy. Based on the orbital structure of the Cu–O bonds, one might expect that it would be necessary to include multiple bands, in order to capture charge transfer from the Cu d orbitals to the neighbouring p orbitals on the oxygen atoms. However, hybridization of the Cu and O orbitals enables a hole to be spread over the four oxygen atoms surrounding a central Cu ion, effectively producing a local singlet state which propagates through the lattice as a unit (Zhang and Rice, 1988). This construction justifies the use of the single-band

Hubbard model.

The t-J model emerges from the strong-U limit of the Hubbard model, and can be obtained from second-order perturbation theory, with the hopping introduced as the perturbation (Gros et al., 1987; Ogata and Fukuyama, 2008; Zhang and Rice, 1988). The Hamiltonian for the microscopic t-J model is given by

$$H = -t\sum_{i\delta\sigma} c^{\dagger}_{i\sigma}c_{i+\delta,\sigma} - \mu\sum_{i\sigma} n_{i\sigma} + \frac{J}{2}\sum_{i\delta}\left[\mathbf{S}_i\cdot\mathbf{S}_{i+\delta} - \frac{1}{4}n_i n_{i+\delta}\right], \tag{3.3}$$

where the new parameter $J \propto t^2/U$ is the exchange interaction strength, and where $\mathbf{S}_i$ is the spin operator for site i. Strictly speaking, because this model is arrived at from the strong-U limit, it must be restricted to states with no double-occupancy of any sites. However, this is a correlation effect which is not captured in the mean-field description, and the constraint is therefore relaxed in the mean-field treatment. The spin operators can be rewritten in terms of the electron creation/annihilation operators by recasting them as ladder operators, with

$$S^{+}_i \equiv c^{\dagger}_{i\uparrow}c_{i\downarrow}, \quad S^{-}_i \equiv c^{\dagger}_{i\downarrow}c_{i\uparrow}, \quad S^{z}_i \equiv \frac{1}{2}\big(n_{i\uparrow} - n_{i\downarrow}\big). \tag{3.4}$$

Then

$$\mathbf{S}_i\cdot\mathbf{S}_{i+\delta} = \frac{1}{2}\big(S^{+}_i S^{-}_{i+\delta} + S^{-}_i S^{+}_{i+\delta}\big) + S^{z}_i S^{z}_{i+\delta}. \tag{3.5}$$

Early mean-field theory studies for the t-J model used a slave-boson approach – a representation in which boson operators represent empty sites (or the spins), and fermion operators represent the spins (or empty sites) – in order to obtain a phase diagram and conditions under which SC could be realized (Jayaprakash et al., 1989). Numerical studies have since demonstrated the stability of d-wave SC at absolute zero for the parameter region of actual experimental interest, and the slave-boson

approach at finite T has provided crossover temperatures for coherent quasiparticle motion, suggesting the onset of SC, with qualitative features of the phase diagram in agreement with the experimental one (Ogata and Fukuyama, 2008).

3.1.1 Mean-Field Decomposition

The mean-field decomposition of the t-J model is outlined in Appendix B. The resulting effective Hamiltonian is

$$\begin{aligned} H_{\text{eff}} &= -\sum_{i\delta\sigma}\left(t+\tau_{i\sigma}^{\delta}\right)c_{i\sigma}^{\dagger}c_{i+\delta,\sigma} - \sum_{i\sigma}\left[\mu-\eta_i+\sigma M_i e^{i\mathbf{Q}_M\cdot\mathbf{r}_i}\right]n_{i\sigma} \\ &+ \sum_{i\delta\sigma}\left\{\Delta_{i\sigma}^{\delta}c_{i,\sigma}^{\dagger}c_{i+\delta,-\sigma}^{\dagger}+\text{H.C.}\right\}, \end{aligned} \tag{3.6}$$

where all quantities and operators have their usual meanings. The quantity $\tau_{i\sigma}^{\delta}$ is the Fock shift, which renormalizes the hopping at site i along direction δ, while η_i is the Hartree shift on site i, which renormalizes the chemical potential. The AF order on site i is represented by M_i, with the sign differences of the local moments between adjacent sites denoted by the exponential term containing the AF ordering vector $\mathbf{Q}_M \equiv \pm\pi\hat{x} \pm \pi\hat{y}$. $\Delta_{i\sigma}^{\delta}$ is the d-wave SC order along the bond direction δ from site i; if all the $\Delta_{i\sigma}^{\hat{x}} = -\Delta_{i\sigma}^{\hat{y}}, \forall i$, this describes the uniform d-wave state.[1] Using the final result of Appendix A as the starting point, the BdG equations are similar in form to those of the π-striped SC stated in equation (2.7), but now take the form:

$$\begin{bmatrix} \hat{\xi}_\sigma - \sigma\hat{M} & \hat{\Delta}_\sigma \\ \hat{\Delta}_{-\sigma}^{*} & -\hat{\xi}_{-\sigma}^{*} - \sigma\hat{M} \end{bmatrix} \begin{pmatrix} u_\sigma^n \\ v_{-\sigma}^n \end{pmatrix} = E_{n\sigma} \begin{pmatrix} u_\sigma^n \\ v_{-\sigma}^n \end{pmatrix}, \tag{3.7}$$

[1] The σ index reflects the fact that the AF order breaks the spin-symmetry of the electron operators, and denotes which spin-block the SC gap occupies.

with

$$\hat{\xi}_\sigma u^n_{i\sigma} \equiv -\sum_\delta \left(t + \tau^\delta_{i\sigma}\right) u^n_{i+\delta,\sigma} - [\mu - \eta_i] u^n_{i\sigma} \tag{3.8}$$

$$\hat{M} u^n_{i\sigma} \equiv M_i e^{i\mathbf{Q}\cdot\mathbf{r}_i} u^n_{i\sigma} \tag{3.9}$$

$$\hat{\Delta}_\sigma v^n_{i,-\sigma} \equiv \sum_\delta \left[\Delta^\delta_{i\sigma} v^n_{i+\delta,-\sigma} + \Delta^\delta_{i-\delta,\sigma} v^n_{i-\delta,-\sigma}\right]. \tag{3.10}$$

After replacing the electron operators with the BdG transform (2.2) and using the superlattice translational symmetry (2.10), the following self-consistent equations for the mean fields are arrived at:

$$\begin{aligned}\Delta^\delta_{i\sigma} = -\sigma \frac{J}{4N_k} \sum_{n\mathbf{k}} \big[& u^n_{i+\delta,\sigma}(\mathbf{k}) v^{n*}_{i,-\sigma}(\mathbf{k}) f_{n\mathbf{k}\sigma} - u^n_{i,-\sigma}(\mathbf{k}) v^{n*}_{i+\delta,\sigma}(\mathbf{k})(1 - f_{n\mathbf{k},-\sigma}) \\ & - u^n_{i+\delta,-\sigma}(\mathbf{k}) v^{n*}_{i\sigma}(\mathbf{k})(1 - f_{n\mathbf{k},-\sigma}) + u^n_{i\sigma}(\mathbf{k}) v^{n*}_{i+\delta,-\sigma}(\mathbf{k}) f_{n\mathbf{k}\sigma} \big]\end{aligned} \tag{3.11}$$

$$\tau^\delta_{i\sigma} = \frac{J}{2N_k} \sum_{n\mathbf{k}} \left[u^{n*}_{i+\delta,-\sigma}(\mathbf{k}) u^n_{i,-\sigma}(\mathbf{k}) f_{n\mathbf{k},-\sigma} + v^n_{i+\delta,-\sigma}(\mathbf{k}) v^{n*}_{i,-\sigma}(\mathbf{k})(1 - f_{n\mathbf{k}\sigma}) \right] \tag{3.12}$$

$$\eta_i = -\frac{J}{4N_k} \sum_{\delta\sigma} \sum_{n\mathbf{k}} \left[|u^n_{i+\delta,\sigma}(\mathbf{k})|^2 f_{n\mathbf{k}\sigma} + |v^n_{i+\delta,\sigma}(\mathbf{k})|^2 (1 - f_{n\mathbf{k},-\sigma}) \right], \tag{3.13}$$

$$\begin{aligned} M_i = -\frac{J}{4N_k} e^{i\mathbf{Q}\cdot\mathbf{r}_i} \sum_{\delta n\mathbf{k}} \big[& |u^n_{i+\delta,\uparrow}(\mathbf{k})|^2 f_{n\mathbf{k}\uparrow} + |v^n_{i+\delta,\uparrow}(\mathbf{k})|^2 (1 - f_{n\mathbf{k}\downarrow}) \\ & - |u^n_{i+\delta,\downarrow}(\mathbf{k})|^2 f_{n\mathbf{k}\downarrow} - |v^n_{i+\delta,\downarrow}(\mathbf{k})|^2 (1 - f_{n\mathbf{k}\uparrow}) \big]. \end{aligned} \tag{3.14}$$

Note that these expressions apply only in the bulk of the superlattice unit cell, and that the position index i ranges only over the sites contained within a single unit cell. If site i is on the boundary, then terms in the above equations which contain $i + \delta$ refer to components of the wavefunction in an adjacent unit cell. Under the transformation $\mathbf{r}_i \to \mathbf{r}_i + \mathbf{R}$ outlined in Section 2.3, these terms can be translated back

into the reference unit cell at the expense of a phase factor in the following fashion:

$$\begin{aligned} u^n_{x+1,y}(\mathbf{k}) &\longrightarrow e^{ik_x N_x} u^n_{x+1-N_x,y}(\mathbf{k}) \\ v^n_{x+1,y}(\mathbf{k}) &\longrightarrow e^{ik_x N_x} v^n_{x+1-N_x,y}(\mathbf{k}), \end{aligned} \tag{3.15}$$

and similarly for $\hat{y}$ terms. That is, if (x, y) is on the boundary of the unit cell at $\mathbf{R}$ then $(x + 1, y)$ would be in the unit cell with $\mathbf{R}' = \mathbf{R} + N_x\hat{x}$, and the site index of the BdG wavefunction component is translated back by N_x lattice constants, while the cell index increases by one.[2]

Finally, a definition is also made for the filling, n, which is the average number of electrons per site:

$$n \equiv \frac{1}{N_s} \sum_{i\sigma} \langle c^\dagger_{i\sigma} c_{i\sigma} \rangle, \tag{3.16}$$

where $N_s = N_x N_y$ is the number of sites in the unit cell. In terms of the BdG transform, and including the superlattice translational symmetry, the filling is given by

$$n = \frac{1}{N_s N_k} \sum_{i\sigma} \sum_{n\mathbf{k}} \Big[|u^n_{i\sigma}(\mathbf{k})|^2 f_{n\mathbf{k}\sigma} + |v^n_{i\sigma}(\mathbf{k})|^2 (1 - f_{n\mathbf{k},-\sigma}) \Big], \tag{3.17}$$

where the index i is once again restricted to a single unit cell.

3.1.2 Free Energy

The free energy, F, is given by the well-known Helmholtz expression

$$F = \langle H \rangle - TS, \tag{3.18}$$

[2]Note that the effective Hamiltonian (2.1) tacitly takes account of translations in the $-\hat{x}$ and $-\hat{y}$ directions by assuming that the SC order is the same for the positive direction as it is for the negative direction along a given bond.

where $\langle H \rangle$ is the internal energy, T is the system temperature, and S is the entropy. All calculations in the present work will take place at $T = 0$, and therefore $\langle H \rangle$ – and hence F – is equivalent to the ground state energy. The free energy is, by construction, minimized by the eigenstates of the mean-field Hamiltonian (3.6). On the other hand, the variational free energy is given by

$$F_{\text{var}}(T = 0) = \langle H \rangle_{\text{MF}}, \tag{3.19}$$

where $\langle H \rangle_{\text{MF}}$ is the expectation value of the t-J Hamiltonian with respect to the eigenstates of the mean-field Hamiltonian (de Gennes, 1966):

$$\langle H \rangle_{\text{MF}} = \frac{1}{Z} \sum_{n} \langle n | H_{\text{tJ}} | n \rangle e^{-\beta E_n}. \tag{3.20}$$

The $|n\rangle$ are the eigenstates with eigenvalue E_n, and are given by $H_{\text{eff}}|n\rangle = E_n|n\rangle$, while the partition function Z is given by

$$Z = \sum_{n} e^{-\beta E_n}. \tag{3.21}$$

Making equation (3.19) stationary allows one to connect the mean-fields of (3.6) with the original microscopic Hamiltonian (3.3), and thereby form the self-consistent equations which ensure that the mean-field decomposition holds.

For the t-J model, using (3.3) and applying the electron operator representation

of the spin operators (refer to Appendix B) gives

$$\begin{aligned}\langle H\rangle_{\rm MF} &= -t\sum_{i\delta\sigma}\langle c^\dagger_{i,\sigma}c_{i+\delta,\sigma}\rangle - \mu\sum_{i\sigma}\langle c^\dagger_{i\sigma}c_{i\sigma}\rangle \\ &- \frac{J}{4}\sum_{i\delta}\Big[\langle c^\dagger_{i,\uparrow}c^\dagger_{i+\delta,\downarrow}c_{i,\downarrow}c_{i+\delta,\uparrow}\rangle_{\rm MF} + \langle c^\dagger_{i,\downarrow}c^\dagger_{i+\delta,\uparrow}c_{i,\uparrow}c_{i+\delta,\downarrow}\rangle_{\rm MF} \\ &\quad + \langle c^\dagger_{i,\uparrow}c^\dagger_{i+\delta,\downarrow}c_{i+\delta,\downarrow}c_{i,\uparrow}\rangle_{\rm MF} + \langle c^\dagger_{i,\downarrow}c^\dagger_{i+\delta,\uparrow}c_{i+\delta,\uparrow}c_{i,\downarrow}\rangle_{\rm MF}\Big]. \quad (3.22)\end{aligned}$$

In order to contend with the four-fermion terms, Wick's theorem is brought to bear, which allows any expectation value of an even number of operators to be written as a sum over all permutations of pair-wise expectation values (de Gennes, 1966). After some algebra, the result for the uniform d-wave state is that

$$\begin{aligned}\langle H\rangle_{\rm MF} &= -\sum_{i\delta\sigma}(t+\tau^\delta_{i\sigma}/2)\langle c^\dagger_{i,\sigma}c_{i+\delta,\sigma}\rangle - \sum_{i\sigma}\big(\mu-\eta_i/2+\sigma M_i e^{i\mathbf{Q}_M\cdot r_i}/2\big)\langle c^\dagger_{i\sigma}c_{i\sigma}\rangle \\ &+ 2\sum_{i\delta}\Delta^\delta_i\langle c^\dagger_{i,\uparrow}c^\dagger_{i+\delta,\downarrow}\rangle. \quad (3.23)\end{aligned}$$

On the other hand, for the π-striped SC state, one finds that

$$\begin{aligned}\langle H\rangle_{\rm MF} &= -\sum_{i\delta\sigma}(t+\tau^\delta_{i\sigma}/2)\langle c^\dagger_{i,\sigma}c_{i+\delta,\sigma}\rangle - \sum_{i\sigma}(\mu-\eta_i/2+\sigma M_i e^{i\mathbf{Q}\cdot r_i}/2)\langle c^\dagger_{i\sigma}c_{i\sigma}\rangle \\ &+ 2\sum_{xy}\Big[\Delta\cos(Q_x x)\langle c^\dagger_{x,y,\uparrow}c^\dagger_{x+1,y,\downarrow}\rangle \\ &\quad - \Delta\cos[Q_x(x-1/2)]\langle c^\dagger_{x,y,\uparrow}c^\dagger_{x,y+1,\downarrow}\rangle\Big]. \quad (3.24)\end{aligned}$$

Calculating these expressions for both the π-striped and uniform d-wave SC cases enables direct comparison of their respective free energies. It is clear on general grounds that the SC gradients at the domain walls along the stripes in the π-striped state will make it more energetically expensive than the uniform case. The comparison of free energies is nevertheless critical, since if there are parameter regions where

the free energy of the π-striped case is close to that of the uniform case, then the application of a magnetic field may tip the balance.

3.2 Method of Calculation

It is now necessary to turn to the question of how the self-consistent calculations must actually be carried out. The calculations in this section are based on code originally written by Amit Ghosal (2002) and Dan Knapp (2005) to do self-consistent BdG calculations in the presence of a magnetic field. The code was revised to perform the calculations with the π-striped superlattice translational symmetry as opposed to the original magnetic translational symmetry, and was heavily revamped to modernize it from Fortran 77 to Fortran 90. An algorithm for evaluating the various order parameters self-consistently under the unit cell formalism of Section 2.3 can be implemented as follows:[3]

- Set J, the target filling $\bar{n}$, and the temperature T.
- Set initial values of the order parameters $\Delta^{\hat{x}}_{i,\text{in}}$, $\Delta^{\hat{y}}_{i,\text{in}}$, $\tau^{\hat{x}}_{i,\text{in}}$, $\tau^{\hat{y}}_{i,\text{in}}$, $\eta_{i,\text{in}}$, and n_{in}.
- Loop over $\mathbf{k}$-space, the reciprocal space of the superlattice unit cells.
  - For $\mathbf{k}$ in the top half of the Brillouin zone ($k_y > 0$), calculate $E_n(\mathbf{k})$ and $(u^n_i(\mathbf{k}), v^n_i(\mathbf{k}))$ from the BdG equations, *e.g.* equation (2.13) for the π-striped state.[4]
  - For $\mathbf{k}$ in the bottom half of the Brillouin zone ($k_y < 0$), swap in the corresponding value from the top half according to the BdG symmetry given by equation (2.12).

[3] Note that AF order is neglected for the present section.

[4] This is accomplished by numerical diagonalization using the LAPACK software package provided by Univ. of Tennessee; Univ. of California, Berkeley; Univ. of Colorado Denver; and NAG Ltd.

  - Calculate the contribution of the given $\mathbf{k}$ to the self-consistent relations: (3.12), (3.13), (3.11), and (3.17).
  - Sum the contributions for all $\mathbf{k}$ at each i to find the real-space forms of the order parameters, $\tau^{\hat{x}}_{i,\text{out}}$ and $\tau^{\hat{y}}_{i,\text{out}}$, $\eta_{i,\text{out}}$, $\Delta^{\hat{x}}_{i,\text{out}}$ and $\Delta^{\hat{y}}_{i,\text{out}}$, and n_{out}.

- Find the maximum differences in the order parameters amongst all of the sites:

$$\begin{aligned}\delta\tau^{\hat{x}} &= \max|\tau^{\hat{x}}_{i,\text{out}} - \tau^{\hat{x}}_{i,\text{in}}|, \quad \delta\tau^{\hat{y}} = \max|\tau^{\hat{y}}_{i,\text{out}} - \tau^{\hat{y}}_{i,\text{in}}|, \quad \delta\eta = \max|\eta_{i,\text{out}} - \eta_{i,\text{in}}|,\\ \delta\Delta^{\hat{x}} &= \max|\Delta^{\hat{x}}_{i,\text{out}} - \Delta^{\hat{x}}_{i,\text{in}}|, \quad \delta\Delta^{\hat{y}} = \max|\Delta^{\hat{y}}_{i,\text{out}} - \Delta^{\hat{y}}_{i,\text{in}}|, \quad \delta n = |n_{\text{out}} - \bar{n}|.\end{aligned}$$

  - For each order parameter X aside from n, if $\delta X \leq \epsilon_X$, where ϵ_X is the convergence criterion for that order parameter, then halt and identify $X_{i,\text{out}}$ as X_i, for each i.
  - If $\delta X > \epsilon_X$, then take $X_{i,\text{in}} \to \alpha X_{i,\text{out}} + (1-\alpha)X_{i,\text{in}}$, again for each i, and return to the third step.[5]
  - For n, if $\delta n \leq \epsilon_n$, the convergence criterion for n, then halt and identify n_{out} with n; otherwise, adjust the bare chemical potential μ according to

$$\mu_{\text{out}} = \mu_{\text{in}} + \frac{\partial\mu}{\partial n}\delta n,$$

    which will force the output filling of the subsequent iteration towards $\bar{n}$.[6]

- Calculate system properties of interest from the converged state, such as the

[5] The purpose of mixing the "old" output $X_{i,\text{in}}$ with the "new" output $X_{i,\text{out}}$ is to partially damp out oscillatory behaviour in the convergence, particularly in parameters which can switch sign from iteration to iteration. However, the parameter α is set to 0.75, which biases the convergence towards the newer output.

[6] The quantity $\partial\mu/\partial n$ is not known at the outset of the calculation and is simply assumed to be unity; it has been observed that alternative values have little effect on the final values of the mean fields, though they can affect the convergence rate.

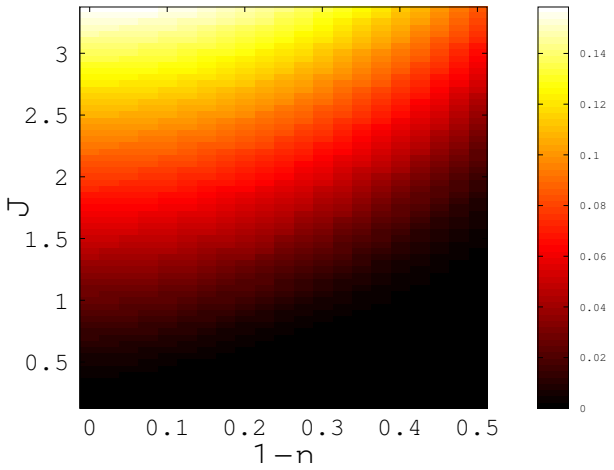

Figure 3.1: A phase diagram of $|\Delta_{\rm av}|$ for a range of values of the doping $(1-n)$ and the strength of the exchange interaction, J. The colourbar indicates the magnitude of $\Delta_{\rm av}$. The region where the d-wave SC is small corresponds approximately to a weakly interacting electron gas, and near half-filling, competition from AF order would produce phase separation were it to be included in the calculation. [$\epsilon_n = 1\times10^{-6}$, $\epsilon_\Delta = 10^{-8}$, $N_{k_x} = N_{k_y} = 2000$; note that there is no superlattice in the uniform case, such that N_k in this case is interpreted as being the same as the number of sites in the lattice.]

DOS and the free energy.

In order to ensure that the code is working correctly for the novel calculations in the π-striped state, it is necessary to apply it to a prototype case with well-understood results. Evaluating the self-consistent equations (3.11)–(3.13) for the uniform d-wave case serves this purpose. The bond-averaged d-wave SC order parameter for a given site is defined by

$$\Delta_{i,\rm av} \equiv \frac{1}{8}\sum_{\delta\sigma}\sigma(-1)^{\delta_y}\Delta^{\delta}_{i\sigma}. \tag{3.25}$$

Taking $J = 1.15t$ and a target filling of $\bar{n} = 7/8$, a value for $|\Delta_{\rm av}|$ of $0.0397t$ was found, which was in agreement within $< 1\%$ of the value obtained at the edge of the magnetic unit cell in Knapp et al. (2005) for the same parameters.

A phase diagram of $|\Delta_{\text{av}}|$ for a range of $(1-n, J)$ values is given in Figure 3.1, and illustrates a decline in the d-wave SC as the filling is lowered at low interaction strength, in good qualitative agreement with the accepted phase diagram for the t-J model (Dagotto, 1994). This region is attributed to a weakly interacting electron gas, which could potentially be understood in the Fermi liquid paradigm, and it therefore stands to reason that mean-field results can do an adequate job of predicting where crossover from the SC state occurs in this regime. On the other hand, near half-filling a complete mean-field treatment would include AF order, which was neglected for the simple uniform-case test. Other computational techniques and high-temperature expansion indicate that AF correlations are strong there, and some form of phase separation occurs (Dagotto, 1994). However, this more complete treatment would necessitate a considerably more elaborate algorithm, and constituted a diversion from the main objective of obtaining results for the uniform case well inside the SC region of the phase diagram, where comparison to the π-striped case is most relevant. AF order was not incorporated into the algorithm for calculating the π-striped SC order self-consistently until initial attempts at convergence without it failed.

3.3 Self-Consistent Equations for the π-Striped Superconductor

In order to determine the stability of the π-striped SC relative to the uniform d-wave state at the mean-field level, it is necessary to find self-consistent equations for the π-striped SC which are analogous to those given in equation (3.11) for the uniform d-wave case. This will necessitate extracting the sinusoidal modulation from the uniform-case pairing expectation values, which is most simply accomplished by Fourier-transforming the electron operators of both the mean-field, effective Hamiltonian for the π-striped SC, equation (2.1), and the mean-field decomposition of the

t-J model, and then matching up the coefficients. This process is carried out in Appendix C.

The resulting self-consistent equation for the π-striped SC order is given by

$$\begin{aligned}\Delta &= -\frac{J}{4N_s}\sum_{x,y}\Big\{\cos\left(Q_x x\right)\Big[\langle c_{x,y,\downarrow}c_{x+1,y,\uparrow}\rangle + \langle c_{x+1,y,\downarrow}c_{x,y,\uparrow}\rangle\Big] \\ &\quad - \cos\left[Q_x(x-1/2)\right]\Big[\langle c_{x,y,\downarrow}c_{x,y+1,\uparrow}\rangle + \langle c_{x,y+1,\downarrow}c_{x,y,\uparrow}\rangle\Big]\Big\}. \quad (3.26)\end{aligned}$$

Note that the sign difference between the $\hat{x}$ and $\hat{y}$ terms reflects the usual sign difference between $\hat{x}$ and $\hat{y}$ parts of the underlying d-wave SC order, which is explicitly taken care of in the mean-field Hamiltonian (2.1). In terms of the BdG transform (2.2), and using the superlattice translational symmetry (2.10), the self-consistent equation becomes

$$\begin{aligned}\Delta &= \frac{J}{4N_sN_{\mathbf{k}}}\sum_{x,y}\sum_{n\mathbf{k}}\Big\{\cos\left(Q_x x\right)\Big[u^n_{x,y}(\mathbf{k})v^{n*}_{x+1,y}(\mathbf{k})(1-2f_{n\mathbf{k}}) \\ &\qquad + u^n_{x+1,y}(\mathbf{k})v^{n*}_{x,y}(\mathbf{k})(1-2f_{n\mathbf{k}})\Big] \\ &\quad - \cos\left[Q_x(x-1/2)\right]\Big[u^n_{x,y}(\mathbf{k})v^{n*}_{x,y+1}(\mathbf{k})(1-2f_{n\mathbf{k}}) \\ &\qquad + u^n_{x,y+1}(\mathbf{k})v^{n*}_{x,y}(\mathbf{k})(1-2f_{n\mathbf{k}})\Big]\Big\}, \quad (3.27)\end{aligned}$$

where the position indices (x, y) are now restricted to range only over a single unit cell, with a phase factor given by (3.15) resulting from crossing the periodic boundary conditions of the unit cell. With this expression, it is possible to attempt to stabilize the π-striped SC at the mean-field level using the algorithm sketched in Section 3.2. The results are presented in the following section.

3.4 Stability of the π-Striped SC at the Mean-Field Level

The analysis of the mean-field stability of the π-striped SC begins with the simplest case, where the π-striped order parameter is determined self-consistently, along with the Hartree shift, η_i, and the Fock shift, $\tau_{i\sigma}^{\delta}$. The algorithm presented in Section 3.2 is applied to the π-striped self-consistent equation (3.27), while equations (3.13) and (3.12) are employed for η_i and $\tau_{i\sigma}^{\delta}$, respectively. For a wide range of interaction strengths J and fillings n, it is found without exception that the magnitude of Δ rapidly falls below the convergence threshold, ϵ_{Δ}. This indicates that the free energy cost associated with SC gradients produced by the modulation is not offset by the reduction offered by the condensation energy; the system would rather adopt the normal state than suffer the SC gradients.

To gain some insight on the nature of this lack of stability, and on what factors might temper it, it is useful to analyze the convergence of the π-striped SC order parameter in terms of a difference equation. Taking the magnitude of the π-striped SC order parameter at a given iteration j of the self-consistent calculation as $\Delta^{(j)}$, then the difference equation which describes the convergence of the modulated SC order is approximately

$$\Delta^{(j+1)} = \alpha^{-1}\Delta^{(j)}, \tag{3.28}$$

with $\alpha > 1$. If one recasts (3.28) as a differential equation by treating the change between subsequent iterations through the finite difference method, then solutions which correspond to (3.28) would have the form of exponential decay, with α as the exponent base, *i.e.* $\Delta^{(j)} = \Delta^{(0)}\alpha^{-j}$. Results which demonstrate this behaviour for the simple starting case are given in Figures 3.2a and 3.2b, for $n = 0.875$ and $n = 1.00$,

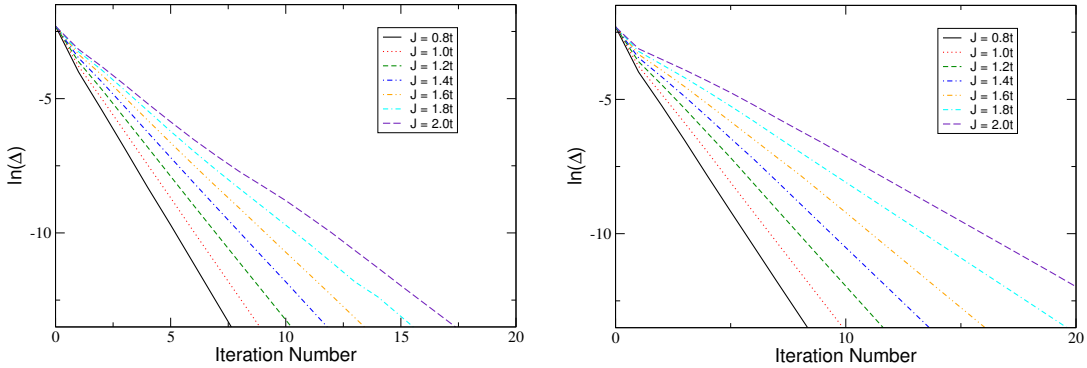

(a) $n = 0.875$ (b) $n = 1.00$

Figure 3.2: Semi-log plots of $\Delta^{(j)}$ convergence rates for 1/8 doping and half-filling, for a series of interaction strengths, and with no AF order. Suppression of the SC order is less pronounced for stronger J, and for the same J at half-filling compared with 1/8 doping. [$\epsilon_\Delta = 10^{-6}$, $N_x = 24$, $N_y = 4$, and $N_{k_x} = N_{k_y} = 24$.]

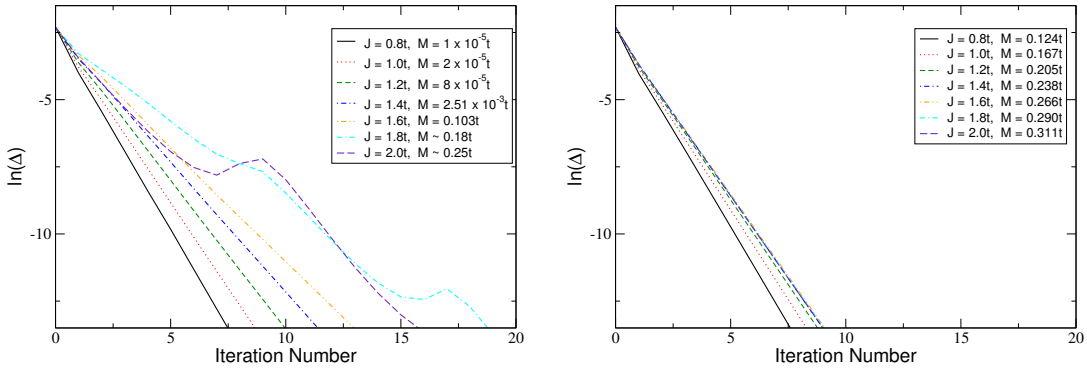

(a) $n = 0.875$, with AF order (b) $n = 1.00$, with AF order

Figure 3.3: Semi-log plots of $\Delta^{(j)}$ convergence rates for 1/8 doping and half-filling, for a series of interaction strengths, but with AF order included. At half-filling, suppression of the SC order is severe, regardless of interaction strength, while at large J for 1/8 doping, the AF order destabilizes the overall convergence. [$\epsilon_\Delta = 10^{-6}$, $N_x = 24$, $N_y = 4$, and $N_{k_x} = N_{k_y} = 24$.]

and for a series of J values. The figures plot the natural logarithm of $\Delta^{(j)}$ as a function of iteration number, j. A straight line with negative slope on these plots corresponds to exponential decay, with the base of the exponent contained in the slope. While both increasing the interaction strength and attempting to stabilize at half-filling (where there is a tendency to order parameter enhancement owing to the presence of a van Hove singularity) do lessen the magnitude of the decay base, the exponential decay is nevertheless always persistent.

As a next step, AF order was introduced into the algorithm of Section 3.2, with the self-consistent equation given by equation (3.14). Variational Monte Carlo (VMC) calculations by Himeda et al. (2002), which have previously suggested that the π-striped state could compete with the uniform state, have also included this order, though with an artificial modulation designed to make it compatible with the PDW modulation. Since AF order arises naturally from the t-J mean-field decomposition (refer to Appendix B), as a first step uniform AF order was incorporated.

Unfortunately, the overall stability of the π-striped state is unchanged by the addition of the AF order, as can be seen in Figures 3.3a and 3.3b, which compare the situation again at 1/8 doping and at half-filling, for a series of J values. While at 1/8 doping the decay base is relatively similarly to that of the simpler case in Figure 3.2a for small J values, contrasting Figures 3.3b and 3.2b indicates that AF order strongly competes with the π-striped state at half-filling (as is also true for the uniform case, as demonstrated in *e.g.* Dagotto (1994)), and actually enhances the rate of SC suppression. This would seem to indicate that future studies including refinements on the straightforward mean-field treatment would probably not need to consider half-filling if there is competing AF order present in the calculation. At larger J for 1/8 doping, the decrease in $\Delta^{(j)}$ is no longer simple exponential decay, although the downward trend is nevertheless clearly evident. The fluctuations in the

SC convergence here are actually driven by the fact that the relatively strong AF order destabilizes the convergence of the Hartree shift Knapp (2005).

It has also been suggested by the VMC calculations of Himeda et al. (2002) that the inclusion of next-nearest neighbour hopping is a key ingredient in stabilizing a modulated SC phase. This is incorporated into the π-striped mean-field Hamiltonian (2.1) by a term of the form

$$-t_1 \sum_{i\delta_1\sigma} c^\dagger_{i\sigma} c_{i+\delta_1,\sigma}, \tag{3.29}$$

which is exactly analogous in form to the original hopping term, but with $t_1 = -0.15t$ as the next-nearest neighbour hopping amplitude, and δ_1 representing all sites which are a distance of $\sqrt{2}a$ from site i, as opposed to a distance of a for the usual nearest-neighbour hopping. The results are presented in Figures 3.4a and 3.4b, which are for 1/8 doping, with the latter also including AF order. The overall trend towards the suppression of the SC order remains, with only a modest change in the decay bases, and the same behaviour occurring for the AF case at large J as seen with only nearest-neighbour hopping in Figure 3.3a. Evidently, while t_1 is a necessary ingredient for stabilization of modulated SC in the VMC calculations, and can also enhance the magnitude of the uniform SC gap, this effect does not carry over to self-consistent BdG calculations.

With the above refinements to the simplest mean-field treatment of the π-striped state proving to be insufficient to stabilize it, the next step was to artificially introduce a modulation of the charge density. By lowering the chemical potential at sites along the domain walls of the PDW stripes, with a compensating increase at all other sites to maintain the same average chemical potential over the whole system, the holes are forced to embed along the nodes of the SC order, and a period-4 CDW

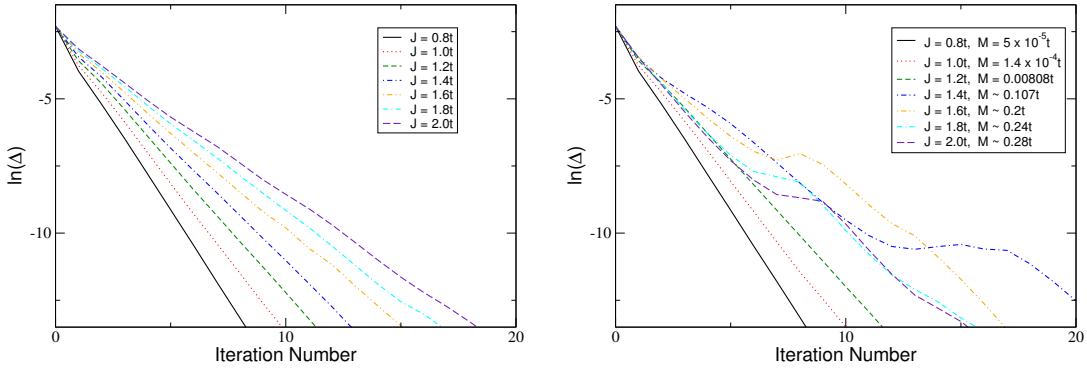

(a) $n = 0.875$, t_1 without AF order (b) $n = 0.875$, t_1 with AF order

Figure 3.4: Semi-log plots of $\Delta^{(j)}$ convergence rates for 1/8 doping and a next-nearest neighbour hopping of $t_1 = -0.15t$, with and without AF order, for a series of interaction strengths. The same trends are observed as for the corresponding cases with only nearest-neighbour hopping. [$\epsilon_\Delta = 10^{-6}$, $N_x = 24$, $N_y = 4$, and $N_{k_x} = N_{k_y} = 24$.]

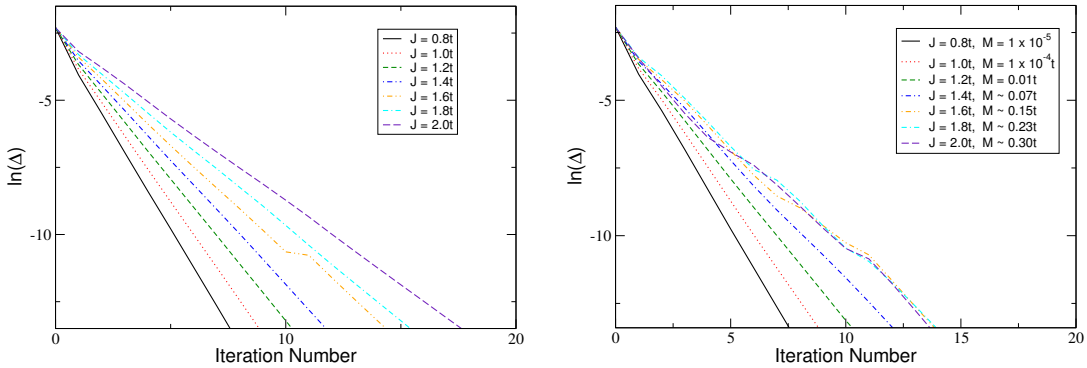

(a) $n = 0.875$, CDW without AF order (b) $n = 0.875$, CDW with AF order

Figure 3.5: Semi-log plots of $\Delta^{(j)}$ convergence rates for 1/8 doping and a CDW induced by a period-4 lowering of the chemical potential by $\delta\mu = -0.5t$, with and without AF order, for a series of interaction strengths. The same trends are observed as for the corresponding cases with only nearest-neighbour hopping. [$\epsilon_\Delta = 10^{-6}$, $N_x = 24$, $N_y = 4$, and $N_{k_x} = N_{k_y} = 24$.]

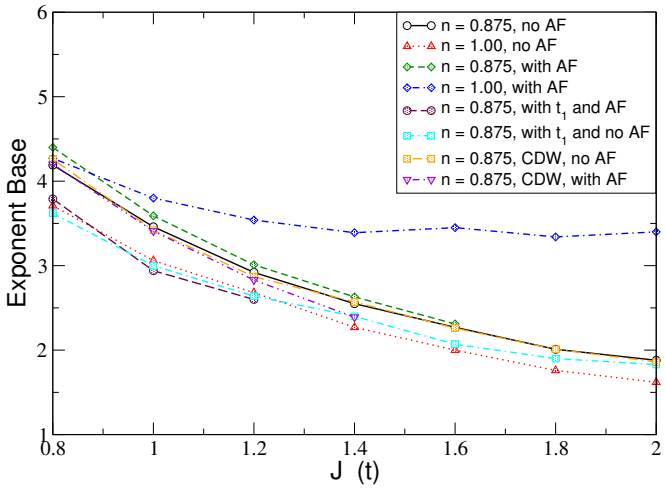

Figure 3.6: A comparison of the decay exponent bases, α, defined in (3.28), for all of the scenarios considered in this section, as a function of the interaction strength. Relevant details of each case are included in the legend. In all cases, $\epsilon_\Delta = 10^{-6}$, $N_x = 24$, $N_y = 4$, and $N_{k_x} = N_{k_y} = 24$.

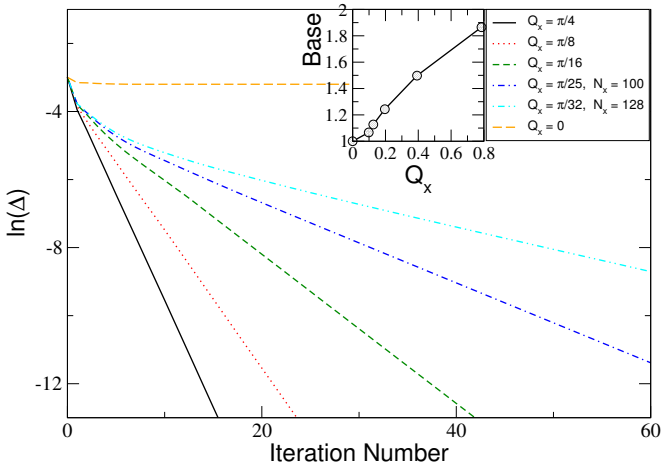

Figure 3.7: Semi-log plot of Δ convergence rates as a function of iteration number for a series of modulations with increasing wavelength. The inset plots the exponent base as a function of Q_x, demonstrating a lack of stability except in the limit of the uniform case. [$\epsilon_\Delta = 10^{-6}$, $N_x = 24$ except where noted, $N_y = 4$, and $N_{k_x} = N_{k_y} = 24$. In all cases $J = 1.4t$.]

commensurate with the PDW is induced. As before, this tactic was also unable to stabilize the π-striped state; the convergence plot is given in Figure 3.5a for the case without AF order. The CDWs in these plots were produced with a lowering of the chemical potential of $\delta\mu = -0.5t$, which induces charge modulations with density decreases of up to 30% at the domain walls for $J = 2.0t$. Different values of $\delta\mu$ did not yield any difference in the convergence of $\Delta^{(j)}$, although they obviously generate CDWs of differing magnitudes (though always with a period of four sites). AF order was also included with the artifical CDW, and the resulting convergence of $\Delta^{(j)}$ is plotted in Figure 3.5b. While the AF order self-consistently adopted the same period-4 modulation as the CDW, it did not enable the SC modulation to become stabilized.

Figure 3.6 summarizes the dependence of the decay base as a function of J for all of the cases considered above. Evidently, the least drastic suppression of the SC order happens at 1/8 doping with next-nearest neighbour hopping, or at half-filling in the absence of competing AF order. These considerations may prove useful in future studies where extensions beyond mean-field theory are incorporated.

One additional angle that was pursued in order to assess the mean-field stability of modulated SC states was to move beyond the restriction to $Q_x = \pi/4$ for the π-striped state. Figure 3.7 shows the convergence rate of $\Delta^{(j)}$ for a series of modulations with increasing wavelength (decreasing Q_x), with the same simple setup as Figures3.2a and 3.2b. While moving to increasingly long wavelengths does result in a progressive reduction in the decay base, it is clear from the inset comparing the sizes of the exponent bases as a function of Q_x that one would have to extrapolate to the long wavelength limit (*i.e.* zero modulation) before one would expect to observe stability. Taken with the above results particular to the π-striped case, this suggests that extensions beyond self-consistent mean-field theory which properly incorporate correlation effects are necessary to realize the π-striped SC state from the microscopic

t-J Hamiltonian.

3.5 Free Energy of the π-Striped SC

One can gain additional insight about the stability of the π-striped phase relative to the normal state by treating Δ as a parameter (*i.e.* without self-consistency) and determining how the variational free energy, F_{var} of (3.24), varies from the normal state case with increasing Δ. In the limit of small Δ near the normal state, Ginzburg-Landau theory can be used to analyze the resulting free energy curves (Tinkham, 2004). For small Δ and in the normal state, a term which is quadratic in the SC order parameter will dominate the expansion, with the free energy minimum occurring for $\Delta = 0$. As the critical point is approached by tuning the parameters of the microscopic Hamiltonian, the curvature of the quadratic term will decrease, until it becomes zero precisely at the critical point, before switching concavity. The coefficient of this quadratic term, which produces this vertical compression, will in general be a complicated function of the parameters of the microscopic Hamiltonian (t, J, and μ), and of the temperature. However, by taking a more phenomenological approach wherein Δ itself is treated like a parameter, the various stabilization scenarios discussed in Section 3.4 can be compared on the basis of the curvature of the free energy curves they produce. This functions as a qualitative measure of "proximity" to the critical point, since lower curvature implies that the coefficient of the quadratic component is closer to zero. In this sense, the curvature of the quadratic component can be viewed as a measure of proximity to a stable π-striped SC state.

The results are presented in Figure 3.8. In all cases, for sufficiently small Δ, parabolic Ginzburg-Landau-type behaviour is observed. The free energy curves have been shifted such that the value of $F_{\text{var}}(\Delta = 0)$, corresponding to the normal state,

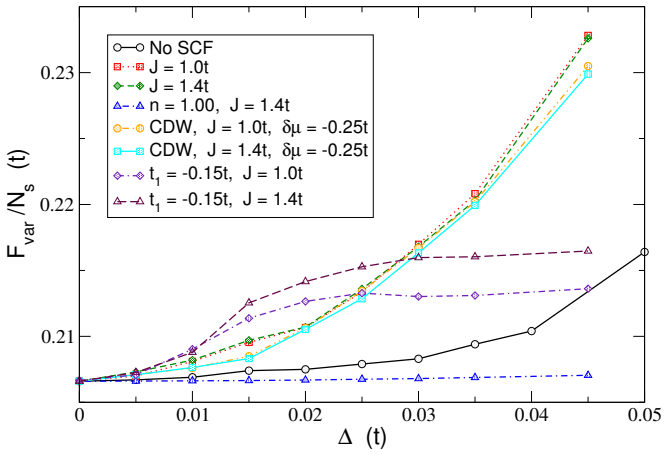

Figure 3.8: Plot of the variational free energy density as a function of the π-striped SC order parameter Δ, which is treated parametrically. Curves for various stabilization scenarios discussed in Section 3.4 are presented, and parabolic Ginzburg-Landau-type behaviour is exhibited for small Δ. Except where noted, all cases correspond to 1/8 doping, and there is no AF present in any case. All curves are shifted such that the normal state energies are the same. [$\epsilon_\Delta = 10^{-6}$, $N_x = 24$, $N_y = 4$, and $N_{k_x} = N_{k_y} = 24$.]

coincides for all cases. The "default" case which provides the benchmark for comparison consists of having no self-consistent treatment at all; the Hartree-Fock shifts are discarded, in addition to fixing Δ. On examining the figure, it is clear that this is actually the most favourable scenario, barring the half-filled case. Evidently then, the Hartree and Fock shifts (which are calculated self-consistently for all other cases besides the default one) can significantly move the system away from the critical point, for sufficiently large J. A modest improvement over the Hartree- and Fock-shifted case is the incorporation of the CDW, at least for moderate values of Δ. The sharpest curvature is observed for the next-nearest hopping cases, with $t_1 = -0.15t$, which also exhibit departure from Ginzburg-Landau physics at the lowest values of Δ. On the other hand, the most favourable case, with the smallest curvature, is for large interaction strength at half-filling. However, it should be noted that this result is obtained in the absence of AF order. As demonstrated in Section 3.4, the

AF order strongly competes with the π-striped SC, which further lowers its stability in the self-consistent calcultions (refer to Figure 3.3b), and so this case is somewhat artificial.[7] Aside from half-filling in the absence of AF order, Figure 3.8 implies that incorporating a CDW by embedding the holes at the SC nodes is the best starting point for further calculations, since this scenario is qualitatively "closest" to the critical point for the onset of the π-striped SC of all of the scenarios examined in this chapter.

[7]Note that for 1/8-doping, the AF order is not strong, even for large J, which is why it is not included in any of the scenarios in Figure 3.8.

Chapter 4

Conclusions

The objective of this thesis was to explore several aspects of the π-striped, d-wave SC within both a phenomenological and a self-consistent BdG theory framework. The former work involved the addition of a CDW order to the phenomenological study of the properties of the π-striped SC in Zelli et al. (2011). It was found that the effect of the CDW is to modestly increase the gap in k-space between the Fermi surface pockets. While this has little qualitative effect on the electronic properties in the absence of a magnetic field, it was found that, for a sufficient strong CDW, the increased gap between the Fermi surface pockets produced substantial degradation in the Landau levels formed by the original phenomenological model. Zelli et al. (2011) observed a similar effect for a large value of the SC order parameter itself, which also disconnects and separates the Fermi surface pockets.

The second and primary objective of this thesis was to treat the π-striped state within self-consistent BdG theory. This involved connecting the phenomenological model of Zelli et al. (2011) with the microscopic t-J model, in order to obtain self-consistent equations for the π-striped order parameter. When these self-consistent equations were evaluated, it was found that the π-striped order was not stable for a range of interaction strengths and doping levels. Various refinements to the Hamiltonian were then included, in order to attempt to stabilize the π-striped state: the

addition of AF order, extension of the hopping to include next-nearest neighbour sites, and the inclusion of a commensurate CDW order. The relative effectiveness of these approaches was compared on the basis of the decay rates of the SC order parameter as a function of iteration number in the self-consistent algorithm. The slowest decay was found at half-filling and strong interaction strength, although the introduction of competing AF order has the opposite effect at this doping level. On the other hand, the CDW order and the next-nearest neighbour hoping yielded slight improvements over the original case. Free energy calculations where the SC order was treated as a parameter and all other mean-fields were evaluated self-consistently were also studied. These confirmed that the CDW order has the lowest free energy increase over the normal state, aside from the artificial cases where the Hartree and Fock shifts are neglected altogether, or where the calculation takes place at half-filling in the absence of competing AF order. Taken together, these preliminary attempts at stabilizing the π-striped SC state from a mean-field treatment of the microscopic t-J model constitute a first step in making the phenomenological results of Zelli et al. (2011) concrete. Future studies can employ the findings of this thesis to determine which refinements to the model are most likely to result in a stable realization of the π-striped state from a microscopic model.

Appendices

Appendix A

Derivation of the BdG Equations

The traditional route to the BdG equations is via the commutator $[c_{i\sigma}, H_{\text{eff}}]$, with H_{eff} given both by (3.6) and by its diagonal form in the quasiparticle basis;

$$H_{\text{eff}} \equiv \sum_{n\sigma} E_{n\sigma}\gamma^{\dagger}_{n\sigma}\gamma_{n\sigma}. \tag{A.1}$$

With both forms of the commutator expressed in terms of the quasiparticle basis, the equality of the two forms produces the BdG equations, as will now be explicitly derived.

Beginning with the commutator obtained directly from (A.1) and using the BdG transform (2.2),

$$\begin{aligned}
[c_{i\sigma}, H_{\text{eff}}] &= \sum_{n} \left[u^{n}_{i\sigma}\gamma_{n\sigma} - \sigma v^{n*}_{i\sigma}\gamma^{\dagger}_{n,-\sigma}\right] \sum_{n'\sigma'} \left[E_{n'\sigma'}\gamma^{\dagger}_{n'\sigma'}\gamma_{n'\sigma'}\right] \\
&\quad - \sum_{n'\sigma'} \left[E_{n'\sigma'}\gamma^{\dagger}_{n'\sigma'}\gamma_{n'\sigma'}\right] \sum_{n} \left[u^{n}_{i\sigma}\gamma_{n\sigma} - \sigma v^{n*}_{i\sigma}\gamma^{\dagger}_{n,-\sigma}\right] \\
&= \sum_{nn'} \sum_{\sigma'} E_{n'\sigma'} \big[u^{n}_{i\sigma}\gamma_{n\sigma}\gamma^{\dagger}_{n'\sigma'}\gamma_{n'\sigma'} - \sigma v^{n*}_{i\sigma}\gamma^{\dagger}_{n,-\sigma}\gamma^{\dagger}_{n'\sigma'}\gamma_{n'\sigma'} \\
&\qquad\qquad - u^{n}_{i\sigma}\gamma^{\dagger}_{n'\sigma'}\gamma_{n'\sigma'}\gamma_{n\sigma} + \sigma v^{n*}_{i\sigma}\gamma^{\dagger}_{n',\sigma'}\gamma_{n'\sigma'}\gamma^{\dagger}_{n,-\sigma}\big].
\end{aligned} \tag{A.2}$$

Applying the quasiparticle commutation relations (2.4) in (A.2),

$$\begin{aligned}
[c_{i\sigma}, H_{\text{eff}}] &= \sum_{nn'} \sum_{\sigma'} E_{n'\sigma'} \Big[u^{n}_{i\sigma}\big(\delta_{n'n}\delta_{\sigma'\sigma} - \gamma^{\dagger}_{n'\sigma'}\gamma_{n\sigma}\big)\gamma_{n'\sigma'} + \sigma v^{n*}_{i\sigma}\gamma^{\dagger}_{n'\sigma'}\gamma^{\dagger}_{n,-\sigma}\gamma_{n'\sigma'} \\
&\qquad\qquad + u^{n}_{i\sigma}\gamma^{\dagger}_{n'\sigma'}\gamma_{n\sigma}\gamma_{n'\sigma'} + \sigma v^{n*}_{i\sigma}\gamma^{\dagger}_{n'\sigma'}\big(\delta_{n'n}\delta_{\sigma'\sigma} - \gamma^{\dagger}_{n,-\sigma}\gamma_{n'\sigma'}\big)\Big] \\
&= \sum_{n'n} \sum_{\sigma'} E_{n'\sigma'} \big[u^{n}_{i\sigma}\gamma_{n'\sigma'}\delta_{n'n}\delta_{\sigma'\sigma} + \sigma v^{n*}_{i\sigma}\gamma^{\dagger}_{n'\sigma'}\delta_{n'n}\delta_{\sigma'\sigma}\big] \\
&= \sum_{n} \big[E_{n\sigma}u^{n}_{i\sigma}\gamma_{n\sigma} + \sigma E_{n,-\sigma}v^{n*}_{i\sigma}\gamma^{\dagger}_{n,-\sigma}\big].
\end{aligned} \tag{A.3}$$

On the other hand, starting from the effective Hamiltonian (3.6), the commutator is

$$\begin{aligned}
[c_{i\sigma}, H_{\text{eff}}] &= -\sum_{i'\delta\sigma'} (t+\tau^{\delta}_{i'\sigma'})\left[c_{i\sigma}c^{\dagger}_{i'\sigma'}c_{i'+\delta,\sigma'} - c^{\dagger}_{i'\sigma'}c_{i'+\delta,\sigma'}c_{i\sigma}\right] \\
&\quad - \sum_{i'\sigma'}\left[\mu - \eta_{i'} + \sigma' M_{i'}e^{i\mathbf{Q}_M\cdot\mathbf{r}_{i'}}\right]\left[c_{i\sigma}c^{\dagger}_{i'\sigma'}c_{i'\sigma'} - c^{\dagger}_{i'\sigma'}c_{i'\sigma'}c_{i\sigma}\right] \\
&\quad + \sum_{i'\delta\sigma'}\Delta^{\delta}_{i'\sigma'}\left[c_{i\sigma}c^{\dagger}_{i'\sigma'}c^{\dagger}_{i'+\delta,-\sigma'} - c^{\dagger}_{i'\sigma'}c^{\dagger}_{i'+\delta,-\sigma'}c_{i\sigma} + c_{i\sigma}c^{\dagger}_{i'+\delta,\sigma'}c^{\dagger}_{i',-\sigma'} - c^{\dagger}_{i'+\delta,\sigma'}c^{\dagger}_{i',-\sigma'}c_{i\sigma}\right],
\end{aligned} \tag{A.4}$$

where it has been noted in the second step that all of the H.C. terms involve products of three annihilation operators, and hence anti-commute and cancel out of $[c_{i\sigma}, H_{\text{eff}}]$. The standard anti-commutation relations for the electron operators can now be applied in (A.4) with the goal of cancelling the negative three-operator term in each of the square parentheses with the result of the anti-commutator for the positive term. Examining each of those terms:

$$c_{i\sigma}c^{\dagger}_{i'\sigma'}c_{i'+\delta,\sigma'} = \left(\delta_{i'i}\delta_{\sigma'\sigma} - c^{\dagger}_{i'\sigma'}c_{i\sigma}\right)c_{i'+\delta,\sigma'} = c_{i'+\delta,\sigma'}\delta_{i'i}\delta_{\sigma'\sigma} + c^{\dagger}_{i'\sigma'}c_{i'+\delta,\sigma'}c_{i\sigma} \tag{A.5}$$

$$c_{i\sigma}c^{\dagger}_{i'\sigma'}c_{i'\sigma'} = \left(\delta_{i'i}\delta_{\sigma'\sigma} - c^{\dagger}_{i'\sigma'}c_{i\sigma}\right)c_{i'\sigma'} = c_{i'\sigma'}\delta_{i'i}\delta_{\sigma'\sigma} + c^{\dagger}_{i'\sigma'}c_{i'\sigma'}c_{i\sigma} \tag{A.6}$$

$$\begin{aligned}
c_{i\sigma}c^{\dagger}_{i'\sigma'}c^{\dagger}_{i'+\delta,-\sigma'} &= \left(\delta_{i'i}\delta_{\sigma'\sigma} - c^{\dagger}_{i'\sigma'}c_{i\sigma}\right)c^{\dagger}_{i'+\delta,-\sigma'} = c^{\dagger}_{i'+\delta,-\sigma'}\delta_{i'i}\delta_{\sigma'\sigma} - c^{\dagger}_{i'\sigma'}\left(\delta_{i'+\delta,i}\delta_{-\sigma',\sigma} - c^{\dagger}_{i'+\delta,-\sigma'}c_{i\sigma}\right) \\
&= c^{\dagger}_{i'+\delta,-\sigma'}\delta_{i'i}\delta_{\sigma'\sigma} - c^{\dagger}_{i'\sigma'}\delta_{i'+\delta,i}\delta_{-\sigma',\sigma} + c^{\dagger}_{i'\sigma'}c^{\dagger}_{i'+\delta,-\sigma'}c_{i\sigma}
\end{aligned} \tag{A.7}$$

$$\begin{aligned}
c_{i\sigma}c^{\dagger}_{i'+\delta,\sigma'}c^{\dagger}_{i',-\sigma'} &= \left(\delta_{i'+\delta,i}\delta_{\sigma'\sigma} - c^{\dagger}_{i'+\delta,\sigma'}c_{i\sigma}\right)c^{\dagger}_{i',-\sigma'} = c^{\dagger}_{i',-\sigma'}\delta_{i'+\delta,i}\delta_{\sigma'\sigma} - c^{\dagger}_{i'+\delta,\sigma'}\left(\delta_{i'i}\delta_{-\sigma',\sigma} - c^{\dagger}_{i',-\sigma'}c_{i\sigma}\right) \\
&= c^{\dagger}_{i',-\sigma'}\delta_{i'+\delta,i}\delta_{\sigma'\sigma} - c^{\dagger}_{i'+\delta,\sigma'}\delta_{i'i}\delta_{-\sigma',\sigma} + c^{\dagger}_{i'+\delta,\sigma'}c^{\dagger}_{i',-\sigma'}c_{i\sigma}
\end{aligned} \tag{A.8}$$

Inserting (A.5)–(A.8) into (A.4) and cancelling the three-operator terms mentioned above gives

$$\begin{aligned}
[c_{i\sigma}, H_{\text{eff}}] &= -\sum_{i'\delta\sigma'}(t+\tau^{\delta}_{i'\sigma'})c_{i'+\delta,\sigma'}\delta_{i'i}\delta_{\sigma'\sigma} - \sum_{i'\sigma'}\left[\mu - \eta_{i'} + \sigma' M_{i'}e^{i\mathbf{Q}_M\cdot\mathbf{r}_{i'}}\right]c_{i'\sigma'}\delta_{i'i}\delta_{\sigma'\sigma} \\
&\quad + \sum_{i'\delta\sigma'}\Delta^{\delta}_{i'\sigma'}\left[c^{\dagger}_{i'+\delta,-\sigma'}\delta_{i'i}\delta_{\sigma'\sigma} - c^{\dagger}_{i'\sigma'}\delta_{i'+\delta,i}\delta_{-\sigma',\sigma} + c^{\dagger}_{i',-\sigma'}\delta_{i'+\delta,i}\delta_{\sigma'\sigma} - c^{\dagger}_{i'+\delta,\sigma'}\delta_{i'i}\delta_{-\sigma',\sigma}\right] \\
&= -\sum_{\delta}(t+\tau^{\delta}_{i\sigma})c_{i+\delta,\sigma} - \left[\mu - \eta_i + \sigma M_i e^{i\mathbf{Q}_M\cdot\mathbf{r}_i}\right]c_{i\sigma} \\
&\quad + \sum_{\delta}\left[\Delta^{\delta}_{i\sigma}c^{\dagger}_{i+\delta,-\sigma} - \Delta^{\delta}_{i-\delta,-\sigma}c^{\dagger}_{i-\delta,-\sigma} + \Delta^{\delta}_{i-\delta,\sigma}c^{\dagger}_{i-\delta,-\sigma} - \Delta^{\delta}_{i,-\sigma}c^{\dagger}_{i+\delta,-\sigma}\right]
\end{aligned} \tag{A.9}$$

However, it is important to realize that the Δ terms in the final line of (A.9) are not all simultaneously realized; the positive ones and the negative ones are mutually exclusive, arising from $\sigma' = \uparrow$ states and $\sigma' = \downarrow$ ones, respectively. This can be compactly summarized as

$$[c_{i\sigma}, H_{\text{eff}}] = -\sum_{\delta}(t+\tau^{\delta}_{i\sigma})c_{i+\delta,\sigma} - \left[\mu - \eta_i + \sigma M_i e^{i\mathbf{Q}_M\cdot\mathbf{r}_i}\right]c_{i\sigma} + \sigma\sum_{\delta}\left[\Delta^{\delta}_{i\sigma}c^{\dagger}_{i+\delta,-\sigma} + \Delta^{\delta}_{i-\delta,\sigma}c^{\dagger}_{i-\delta,-\sigma}\right]. \tag{A.10}$$

Applying the BdG transform (2.2) in (A.10) gives

$$\begin{aligned}
[c_{i\sigma}, H_{\text{eff}}] &= -\sum_{\delta}(t+\tau_{i\sigma}^{\delta})\sum_{n}[u_{i+\delta,\sigma}^{n}\gamma_{n\sigma}^{\dagger} - \sigma v_{i+\delta,\sigma}^{n*}\gamma_{n,-\sigma}^{\dagger}] \\
&\quad - [\mu - \eta_i + \sigma M_i e^{i\mathbf{Q}_M\cdot\mathbf{r}_i}]\sum_{n}[u_{i\sigma}^{n}\gamma_{n\sigma} - \sigma v_{i\sigma}^{n*}\gamma_{n,-\sigma}^{\dagger}] \\
&\quad + \sigma\sum_{\delta}\Delta_{i\sigma}^{\delta}\sum_{n}[u_{i+\delta,-\sigma}^{n*}\gamma_{n,-\sigma}^{\dagger} + \sigma v_{i+\delta,-\sigma}^{n}\gamma_{n\sigma}] \\
&\quad + \sigma\sum_{\delta}\Delta_{i-\delta,\sigma}^{\delta}\sum_{n}[u_{i-\delta,-\sigma}^{n*}\gamma_{n,-\sigma}^{\dagger} + \sigma v_{i-\delta,-\sigma}^{n}\gamma_{n\sigma}] \\
&= -\sum_{\delta}(t+\tau_{i\sigma}^{\delta})\sum_{n}u_{i+\delta,\sigma}^{n}\gamma_{n\sigma} - [\mu - \eta_i + \sigma M_i e^{i\mathbf{Q}_M\cdot\mathbf{r}_i}]\sum_{n}u_{i\sigma}^{n}\gamma_{n\sigma} \\
&\quad + \sigma^2\sum_{\delta}\sum_{n}[\Delta_{i\sigma}^{\delta}v_{i+\delta,-\sigma}^{n}\gamma_{n\sigma} + \Delta_{i-\delta,\sigma}^{\delta}v_{i-\delta,-\sigma}^{n}\gamma_{n\sigma}] \\
&\quad + \sigma\sum_{\delta}(t+\tau_{i\sigma}^{\delta})\sum_{n}v_{i+\delta,\sigma}^{n*}\gamma_{n,-\sigma}^{\dagger} + \sigma[\mu-\eta_i]\sum_{n}v_{i\sigma}^{n*}\gamma_{n,-\sigma}^{\dagger} \\
&\quad + \sigma\sum_{\delta}\sum_{n}[\Delta_{i\sigma}^{\delta}u_{i+\delta,-\sigma}^{n*}\gamma_{n,-\sigma}^{\dagger} + \Delta_{i-\delta,\sigma}^{\delta}u_{i-\delta,-\sigma}^{n*}\gamma_{n,-\sigma}^{\dagger}].
\end{aligned} \tag{A.11}$$

Equating (A.3) and (A.11) gives

$$\begin{aligned}
E_{n\sigma}u_{i\sigma}^{n}\gamma_{n\sigma} + \sigma E_{n,-\sigma}v_{i\sigma}^{n*}\gamma_{n,-\sigma}^{\dagger} &= \\
\Big\{-\sum_{\delta}(t+\tau_{i\sigma}^{\delta})u_{i+\delta,\sigma}^{n} - [\mu-\eta_i+\sigma M_i e^{i\mathbf{Q}_M\cdot\mathbf{r}_i}]u_{i\sigma}^{n} &+ \sum_{\delta}[\Delta_{i\sigma}^{\delta}v_{i+\delta,-\sigma}^{n} + \Delta_{i-\delta,\sigma}^{\delta}v_{i-\delta,-\sigma}^{n}]\Big\}\gamma_{n\sigma} \\
+\Big\{\sigma\sum_{\delta}(t+\tau_{i\sigma}^{\delta})v_{i+\delta,\sigma}^{n*} + \sigma[\mu-\eta_i]v_{i\sigma}^{n*} &+ \sigma\sum_{\delta}[\Delta_{i\sigma}^{\delta}u_{i+\delta,-\sigma}^{n*} + \Delta_{i-\delta,\sigma}^{\delta}u_{i-\delta,-\sigma}^{n*}]\Big\}\gamma_{n,-\sigma}^{\dagger}.
\end{aligned} \tag{A.12}$$

Since the quasiparticle operators constitute a complete set, and are therefore linearly independent, equation (A.12) can be separated into two equations:

$$\begin{aligned}
E_{n\sigma}u_{i\sigma}^{n} &= -\sum_{\delta}(t+\tau_{i\sigma}^{\delta})u_{i+\delta,\sigma}^{n} - [\mu-\eta_i+\sigma M_i e^{i\mathbf{Q}_M\cdot\mathbf{r}_i}]u_{i\sigma}^{n} + \sum_{\delta}[\Delta_{i\sigma}^{\delta}v_{i+\delta,-\sigma}^{n} + \Delta_{i-\delta,\sigma}^{\delta}v_{i-\delta,-\sigma}^{n}] \\
\sigma E_{n,-\sigma}v_{i\sigma}^{n*} &= \sigma\sum_{\delta}(t+\tau_{i\sigma}^{\delta})v_{i+\delta,\sigma}^{n*} + \sigma[\mu-\eta_i+\sigma M_i e^{i\mathbf{Q}_M\cdot\mathbf{r}_i}]v_{i\sigma}^{n*} + \sigma\sum_{\delta}[\Delta_{i\sigma}^{\delta}u_{i+\delta,-\sigma}^{n*} + \Delta_{i-\delta,\sigma}^{\delta}u_{i-\delta,-\sigma}^{n*}].
\end{aligned} \tag{A.13}$$

Finally, multiplying the second of equations (A.13) by σ and taking the complex conjugate, one arrives at the first pair of BdG equations:

$$\begin{aligned}
E_{n\sigma}u_{i\sigma}^{n} &= -\sum_{\delta}(t+\tau_{i\sigma}^{\delta})u_{i+\delta,\sigma}^{n} - [\mu-\eta_i+\sigma M_i e^{i\mathbf{Q}_M\cdot\mathbf{r}_i}]u_{i\sigma}^{n} + \sum_{\delta}[\Delta_{i\sigma}^{\delta}v_{i+\delta,-\sigma}^{n} + \Delta_{i-\delta,\sigma}^{\delta}v_{i-\delta,-\sigma}^{n}] \\
E_{n,-\sigma}v_{i\sigma}^{n} &= +\sum_{\delta}(t+\tau_{i\sigma}^{\delta *})v_{i+\delta,\sigma}^{n} + [\mu-\eta_i+\sigma M_i e^{i\mathbf{Q}_M\cdot\mathbf{r}_i}]v_{i\sigma}^{n} + \sum_{\delta}[\Delta_{i\sigma}^{\delta *}u_{i+\delta,-\sigma}^{n} + \Delta_{i-\delta,\sigma}^{\delta *}u_{i-\delta,-\sigma}^{n}].
\end{aligned} \tag{A.14}$$

The pair of equations (A.14) links the states with $E_{n\sigma}$ to states with $E_{n,-\sigma}$; in order to solve for one of these eigenvalues, it is necessary to construct the complementary set of equations stemming from $[c_{i,-\sigma}, H_{\text{eff}}]$. By following through the process given

above, one finds that

$$[c_{i,-\sigma}, H_{\text{eff}}] = \sum_n \left[E_{n,-\sigma} u^n_{i,-\sigma} \gamma_{n,-\sigma} - \sigma E_{n\sigma} v^{n*}_{i,-\sigma} \gamma^\dagger_{n\sigma} \right] \tag{A.15}$$

and

$$[c_{i,-\sigma}, H_{\text{eff}}] = -\sum_\delta (t + \tau^\delta_{i,-\sigma}) c_{i+\delta,-\sigma} - [\mu - \eta_i - \sigma M_i e^{i\mathbf{Q}_M \cdot \mathbf{r}_i}] c_{i,-\sigma} - \sigma \sum_\delta [\Delta^\delta_{i,-\sigma} c^\dagger_{i+\delta,\sigma} + \Delta^\delta_{i-\delta,-\sigma} c^\dagger_{i-\delta,\sigma}]. \tag{A.16}$$

These, in turn, lead to the complementary pair of BdG equations:

$$\begin{aligned} E_{n,-\sigma} u^n_{i,-\sigma} &= -\sum_\delta (t + \tau^\delta_{i,-\sigma}) u^n_{i+\delta,-\sigma} - [\mu - \eta_i - \sigma M_i e^{i\mathbf{Q}_M \cdot \mathbf{r}_i}] u^n_{i,-\sigma} + \sum_\delta [\Delta^\delta_{i,-\sigma} v^n_{i+\delta,\sigma} + \Delta^\delta_{i-\delta,-\sigma} v^n_{i-\delta,\sigma}] \\ E_{n\sigma} v^n_{i,-\sigma} &= \sum_\delta (t + \tau^{\delta*}_{i,-\sigma}) v^n_{i+\delta,-\sigma} + [\mu - \eta_i - \sigma M_i e^{i\mathbf{Q}_M \cdot \mathbf{r}_i}] v^n_{i,-\sigma} + \sum_\delta [\Delta^{\delta*}_{i,-\sigma} u^n_{i+\delta,\sigma} + \Delta^{\delta*}_{i-\delta,-\sigma} u^n_{i-\delta,\sigma}]. \end{aligned} \tag{A.17}$$

The two equations for $E_{n\sigma}$, from (A.14) and (A.17), can now be combined, giving the final form of the BdG equations:

$$\begin{aligned} E_{n\sigma} u^n_{i\sigma} &= -\sum_\delta (t + \tau^\delta_{i\sigma}) u^n_{i+\delta,\sigma} - [\mu - \eta_i + \sigma M_i e^{i\mathbf{Q}_M \cdot \mathbf{r}_i}] u^n_{i\sigma} + \sum_\delta [\Delta^\delta_{i\sigma} v^n_{i+\delta,-\sigma} + \Delta^\delta_{i-\delta,\sigma} v^n_{i-\delta,-\sigma}] \\ E_{n\sigma} v^n_{i,-\sigma} &= \sum_\delta (t + \tau^{\delta*}_{i,-\sigma}) v^n_{i+\delta,-\sigma} + [\mu - \eta_i - \sigma M_i e^{i\mathbf{Q}_M \cdot \mathbf{r}_i}] v^n_{i,-\sigma} + \sum_\delta [\Delta^{\delta*}_{i,-\sigma} u^n_{i+\delta,\sigma} + \Delta^{\delta*}_{i-\delta,-\sigma} u^n_{i-\delta,\sigma}]. \end{aligned} \tag{A.18}$$

Appendix B

Mean-Field Decomposition of the t-J Model

The Hamiltonian for the t-J model on a square lattice is given by equation (3.3):

$$H = -t \sum_{i\delta\sigma} c^\dagger_{i\sigma} c_{i+\delta,\sigma} + \frac{J}{2} \sum_{i\delta} \left[\mathbf{S}_i \cdot \mathbf{S}_{i+\delta} - \frac{1}{4} n_i n_{i+\delta} \right] - \mu \sum_{i\sigma} n_{i\sigma}. \tag{B.1}$$

Defining $d_{i\uparrow} \equiv c^\dagger_{i\uparrow} c_{i\uparrow} - \langle c^\dagger_{i\uparrow} c_{i\uparrow} \rangle$ and $d_{i\downarrow} \equiv c^\dagger_{i\downarrow} c_{i\downarrow} - \langle c^\dagger_{i\downarrow} c_{i\downarrow} \rangle$, then their product is

$$d_{i\uparrow} d_{i\downarrow} = c^\dagger_{i\uparrow} c_{i\uparrow} c^\dagger_{i\downarrow} c_{i\downarrow} - \langle c^\dagger_{i\downarrow} c_{i\downarrow} \rangle c^\dagger_{i\uparrow} c_{i\uparrow} - \langle c^\dagger_{i\uparrow} c_{i\uparrow} \rangle c^\dagger_{i\downarrow} c_{i\downarrow} + \langle c^\dagger_{i\uparrow} c_{i\uparrow} \rangle \langle c^\dagger_{i\downarrow} c_{i\downarrow} \rangle. \tag{B.2}$$

Rearranging (B.2),

$$\begin{aligned} c^\dagger_{i\uparrow} c_{i\uparrow} c^\dagger_{i\downarrow} c_{i\downarrow} &= d_{i\uparrow} d_{i\downarrow} + \langle c^\dagger_{i\downarrow} c_{i\downarrow} \rangle c^\dagger_{i\uparrow} c_{i\uparrow} + \langle c^\dagger_{i\uparrow} c_{i\uparrow} \rangle c^\dagger_{i\downarrow} c_{i\downarrow} - \langle c^\dagger_{i\uparrow} c_{i\uparrow} \rangle \langle c^\dagger_{i\downarrow} c_{i\downarrow} \rangle \\ &\approx \langle c^\dagger_{i\downarrow} c_{i\downarrow} \rangle c^\dagger_{i\uparrow} c_{i\uparrow} + \langle c^\dagger_{i\uparrow} c_{i\uparrow} \rangle c^\dagger_{i\downarrow} c_{i\downarrow} - \langle c^\dagger_{i\uparrow} c_{i\uparrow} \rangle \langle c^\dagger_{i\downarrow} c_{i\downarrow} \rangle, \end{aligned} \tag{B.3}$$

where the approximation is to disregard the square of the difference between the operator $c^\dagger_{i\sigma} c_{i\sigma}$ and its average value. One could similarly take the permutation $c^\dagger_{i\uparrow} c_{i\uparrow} c^\dagger_{i\downarrow} c_{i\downarrow} = -c^\dagger_{i\uparrow} c_{i\downarrow} c^\dagger_{i\downarrow} c_{i\uparrow}$ and decompose it in the same fashion, but this would imply a spin-flip scattering mechanism which is presumably absent in the present model. Finally, there exists the permutation $c^\dagger_{i\uparrow} c_{i\uparrow} c^\dagger_{i\downarrow} c_{i\downarrow} = c^\dagger_{i\uparrow} c^\dagger_{i\downarrow} c_{i\downarrow} c_{i\uparrow}$. Taking $d_{\uparrow\downarrow} \equiv c^\dagger_{i\uparrow} c^\dagger_{i\downarrow} - \langle c^\dagger_{i\uparrow} c^\dagger_{i\downarrow} \rangle$ and $d_{\downarrow\uparrow} \equiv c_{i\downarrow} c_{i\uparrow} - \langle c_{i\downarrow} c_{i\uparrow} \rangle$, then as above,

$$\begin{aligned} d_{\uparrow\downarrow} d_{\downarrow\uparrow} &= c^\dagger_{i\uparrow} c^\dagger_{i\downarrow} c_{i\downarrow} c_{i\uparrow} - \langle c_{i\downarrow} c_{i\uparrow} \rangle c^\dagger_{i\uparrow} c^\dagger_{i\downarrow} - \langle c^\dagger_{i\uparrow} c^\dagger_{i\downarrow} \rangle c_{i\downarrow} c_{i\uparrow} + \langle c^\dagger_{i\uparrow} c^\dagger_{i\downarrow} \rangle \langle c_{i\downarrow} c_{i\downarrow} \rangle \\ \implies \quad c^\dagger_{i\uparrow} c^\dagger_{i\downarrow} c_{i\downarrow} c_{i\uparrow} &\approx \langle c_{i\downarrow} c_{i\uparrow} \rangle c^\dagger_{i\uparrow} c^\dagger_{i\downarrow} + \langle c^\dagger_{i\uparrow} c^\dagger_{i\downarrow} \rangle c_{i\downarrow} c_{i\uparrow} - \langle c^\dagger_{i\uparrow} c^\dagger_{i\downarrow} \rangle \langle c_{i\downarrow} c_{i\downarrow} \rangle. \end{aligned} \tag{B.4}$$

This decomposition produces mean-field electron pairing terms, and hence, superconductivity.

For the exchange term in (3.3), the spin operators can be rewritten in terms of

the electron creation/annihilation operators by recasting them as ladder operators, with

$$S_i^+ \equiv c_{i\uparrow}^\dagger c_{i\downarrow}, \quad S_i^- \equiv c_{i\downarrow}^\dagger c_{i\uparrow}, \quad S_i^z \equiv \frac{1}{2}\big(n_{i\uparrow} - n_{i\downarrow}\big). \tag{B.5}$$

Then

$$\begin{aligned}
\frac{J}{2}\sum_{i\delta}\Big[\mathbf{S}_i\cdot\mathbf{S}_{i+\delta} \;-\; \tfrac{1}{4}n_i n_{i+\delta}\Big] &= \frac{J}{2}\sum_{i\delta}\Big[\frac{1}{2}(S_i^+S_{i+\delta}^- + S_i^-S_{i+\delta}^+) + S_i^zS_{i+\delta}^z - \frac{1}{4}n_in_{i+\delta}\Big] \\
&= \frac{J}{2}\sum_{i\delta}\Big[\frac{1}{2}(c_{i\uparrow}^\dagger c_{i\downarrow}c_{i+\delta,\downarrow}^\dagger c_{i+\delta,\uparrow} + c_{i\downarrow}^\dagger c_{i\uparrow}c_{i+\delta,\uparrow}^\dagger c_{i+\delta,\downarrow}) \\
&\quad + \frac{1}{4}\big(n_{i\uparrow}-n_{i\downarrow}\big)\big(n_{i+\delta,\uparrow}-n_{i+\delta,\downarrow}\big) - \frac{1}{4}\big(n_{i\uparrow}+n_{i\downarrow}\big)\big(n_{i+\delta,\uparrow}+n_{i+\delta,\downarrow}\big)\Big] \\
&= \frac{J}{2}\sum_{i\delta}\Big[\frac{1}{2}(c_{i\uparrow}^\dagger c_{i\downarrow}c_{i+\delta,\downarrow}^\dagger c_{i+\delta,\uparrow} + c_{i\downarrow}^\dagger c_{i\uparrow}c_{i+\delta,\uparrow}^\dagger c_{i+\delta,\downarrow}) \\
&\qquad + \frac{1}{4}\big(n_{i\uparrow}n_{i+\delta,\uparrow} - n_{i\uparrow}n_{i+\delta,\downarrow} - n_{i\downarrow}n_{i+\delta,\uparrow} + n_{i\downarrow}n_{i+\delta,\downarrow} \\
&\qquad - n_{i\uparrow}n_{i+\delta,\uparrow} - n_{i\uparrow}n_{i+\delta,\downarrow} - n_{i\downarrow}n_{i+\delta,\uparrow} - n_{i\downarrow}n_{i+\delta,\downarrow}\big)\Big] \\
&= \frac{J}{2}\sum_{i\delta}\Big[\frac{1}{2}(c_{i\uparrow}^\dagger c_{i\downarrow}c_{i+\delta,\downarrow}^\dagger c_{i+\delta,\uparrow} + c_{i\downarrow}^\dagger c_{i\uparrow}c_{i+\delta,\uparrow}^\dagger c_{i+\delta,\downarrow}) - \frac{1}{2}n_{i\uparrow}n_{i+\delta,\downarrow} - \frac{1}{2}n_{i\downarrow}n_{i+\delta,\uparrow}\Big] \\
&= \frac{J}{4}\sum_{i\delta}\Big[-c_{i\uparrow}^\dagger c_{i+\delta,\downarrow}^\dagger c_{i\downarrow}c_{i+\delta,\uparrow} - c_{i\downarrow}^\dagger c_{i+\delta,\uparrow}^\dagger c_{i\uparrow}c_{i+\delta,\downarrow} - c_{i\uparrow}^\dagger c_{i\uparrow}c_{i+\delta,\downarrow}^\dagger c_{i+\delta,\downarrow} - c_{i\downarrow}^\dagger c_{i\downarrow}c_{i+\delta,\uparrow}^\dagger c_{i+\delta,\uparrow}\Big] \\
&= -\frac{J}{4}\sum_{i\delta}\Big[c_{i\uparrow}^\dagger c_{i+\delta,\downarrow}^\dagger c_{i\downarrow}c_{i+\delta,\uparrow} + c_{i\downarrow}^\dagger c_{i+\delta,\uparrow}^\dagger c_{i\uparrow}c_{i+\delta,\downarrow} + c_{i\uparrow}^\dagger c_{i+\delta,\downarrow}^\dagger c_{i+\delta,\downarrow}c_{i\uparrow} + c_{i\downarrow}^\dagger c_{i+\delta,\uparrow}^\dagger c_{i+\delta,\uparrow}c_{i\downarrow}\Big]
\end{aligned} \tag{B.6}$$

Referring back to (B.3) and (B.4), the four-fermion terms in (B.6) can be decoupled as follows:

$$\begin{aligned}
c_{i\uparrow}^\dagger c_{i+\delta,\downarrow}^\dagger c_{i\downarrow}c_{i+\delta,\uparrow} &\approx \langle c_{i\uparrow}^\dagger c_{i+\delta,\downarrow}^\dagger\rangle c_{i\downarrow}c_{i+\delta,\uparrow} + \langle c_{i\downarrow}c_{i+\delta,\uparrow}\rangle c_{i\uparrow}^\dagger c_{i+\delta,\downarrow}^\dagger - \langle c_{i\uparrow}^\dagger c_{i+\delta,\downarrow}^\dagger\rangle\langle c_{i\downarrow}c_{i+\delta,\uparrow}\rangle \\
&\quad + \langle c_{i\uparrow}^\dagger c_{i+\delta,\uparrow}\rangle c_{i+\delta,\downarrow}^\dagger c_{i\downarrow} + \langle c_{i+\delta,\downarrow}^\dagger c_{i\downarrow}\rangle c_{i\uparrow}^\dagger c_{i+\delta,\uparrow} - \langle c_{i\uparrow}^\dagger c_{i+\delta,\uparrow}\rangle\langle c_{i+\delta,\downarrow}^\dagger c_{i\downarrow}\rangle \\
c_{i\downarrow}^\dagger c_{i+\delta,\uparrow}^\dagger c_{i\uparrow}c_{i+\delta,\downarrow} &\approx \langle c_{i\downarrow}^\dagger c_{i+\delta,\uparrow}^\dagger\rangle c_{i\uparrow}c_{i+\delta,\downarrow} + \langle c_{i\uparrow}c_{i+\delta,\downarrow}\rangle c_{i\downarrow}^\dagger c_{i+\delta,\uparrow}^\dagger - \langle c_{i\downarrow}^\dagger c_{i+\delta,\uparrow}^\dagger\rangle\langle c_{i\uparrow}c_{i+\delta,\downarrow}\rangle \\
&\quad + \langle c_{i\downarrow}^\dagger c_{i+\delta,\downarrow}\rangle c_{i+\delta,\uparrow}^\dagger c_{i\uparrow} + \langle c_{i+\delta,\uparrow}^\dagger c_{i\uparrow}\rangle c_{i\downarrow}^\dagger c_{i+\delta,\downarrow} - \langle c_{i\downarrow}^\dagger c_{i+\delta,\downarrow}\rangle\langle c_{i+\delta,\uparrow}^\dagger c_{i\uparrow}\rangle \\
c_{i\uparrow}^\dagger c_{i+\delta,\downarrow}^\dagger c_{i+\delta,\downarrow}c_{i\uparrow} &\approx \langle c_{i\uparrow}^\dagger c_{i+\delta,\downarrow}^\dagger\rangle c_{i+\delta,\downarrow}c_{i\uparrow} + \langle c_{i+\delta,\downarrow}c_{i\uparrow}\rangle c_{i\uparrow}^\dagger c_{i+\delta,\downarrow}^\dagger - \langle c_{i\uparrow}^\dagger c_{i+\delta,\downarrow}^\dagger\rangle\langle c_{i+\delta,\downarrow}c_{i\uparrow}\rangle \\
&\quad + \langle c_{i\uparrow}^\dagger c_{i\uparrow}\rangle c_{i+\delta,\downarrow}^\dagger c_{i+\delta,\downarrow} + \langle c_{i+\delta,\downarrow}^\dagger c_{i+\delta,\downarrow}\rangle c_{i\uparrow}^\dagger c_{i\uparrow} - \langle c_{i\uparrow}^\dagger c_{i\uparrow}\rangle\langle c_{i+\delta,\downarrow}^\dagger c_{i+\delta,\downarrow}\rangle \\
c_{i\downarrow}^\dagger c_{i+\delta,\uparrow}^\dagger c_{i+\delta,\uparrow}c_{i\downarrow} &\approx \langle c_{i\downarrow}^\dagger c_{i+\delta,\uparrow}^\dagger\rangle c_{i+\delta,\uparrow}c_{i\downarrow} + \langle c_{i+\delta,\uparrow}c_{i\downarrow}\rangle c_{i\downarrow}^\dagger c_{i+\delta,\uparrow}^\dagger - \langle c_{i\downarrow}^\dagger c_{i+\delta,\uparrow}^\dagger\rangle\langle c_{i+\delta,\uparrow}c_{i\downarrow}\rangle \\
&\quad + \langle c_{i\downarrow}^\dagger c_{i\downarrow}\rangle c_{i+\delta,\uparrow}^\dagger c_{i+\delta,\uparrow} + \langle c_{i+\delta,\uparrow}^\dagger c_{i+\delta,\uparrow}\rangle c_{i\downarrow}^\dagger c_{i\downarrow} - \langle c_{i\downarrow}^\dagger c_{i\downarrow}\rangle\langle c_{i+\delta,\uparrow}^\dagger c_{i+\delta,\uparrow}\rangle
\end{aligned} \tag{B.7}$$

Applying (B.7) in (B.6), the decoupled terms are grouped according to function into: (*i*) SC terms, (*ii*) Fock shift (FS) terms, (*iii*) Hartree shift (HS) terms, and (*iv*) constant terms for the shifts, C_{shift}, and the pairing, C_{pair}. That is,

$$\text{SC} = -\frac{J}{4}\sum_{i\delta}\Big[\langle c_{i\downarrow}c_{i+\delta,\uparrow}\rangle c_{i\uparrow}^\dagger c_{i+\delta,\downarrow}^\dagger + \langle c_{i\uparrow}c_{i+\delta,\downarrow}\rangle c_{i\downarrow}^\dagger c_{i+\delta,\uparrow}^\dagger + \langle c_{i+\delta,\downarrow}c_{i\uparrow}\rangle c_{i\uparrow}^\dagger c_{i+\delta,\downarrow}^\dagger + \langle c_{i+\delta,\uparrow}c_{i\downarrow}\rangle c_{i\downarrow}^\dagger c_{i+\delta,\uparrow}^\dagger + \text{H.C.}\Big] \tag{B.8}$$

$$C_{\text{pair}} = +\frac{J}{4}\sum_{i\delta}\Big[\langle c^\dagger_{i\uparrow}c^\dagger_{i+\delta,\downarrow}\rangle\langle c_{i\downarrow}c_{i+\delta,\uparrow}\rangle + \langle c^\dagger_{i\downarrow}c^\dagger_{i+\delta,\uparrow}\rangle\langle c_{i\uparrow}c_{i+\delta,\downarrow}\rangle + \langle c^\dagger_{i\uparrow}c^\dagger_{i+\delta,\downarrow}\rangle\langle c_{i+\delta,\downarrow}c_{i\uparrow}\rangle + \langle c^\dagger_{i\downarrow}c^\dagger_{i+\delta,\uparrow}\rangle\langle c_{i+\delta,\uparrow}c_{i\downarrow}\rangle\Big] \quad \text{(B.9)}$$

$$\text{FS} = -\frac{J}{4}\sum_{i\delta}\Big[\langle c^\dagger_{i\uparrow}c_{i+\delta,\uparrow}\rangle c^\dagger_{i+\delta,\downarrow}c_{i\downarrow} + \langle c^\dagger_{i+\delta,\downarrow}c_{i\downarrow}\rangle c^\dagger_{i\uparrow}c_{i+\delta,\uparrow} + \langle c^\dagger_{i\downarrow}c_{i+\delta,\downarrow}\rangle c^\dagger_{i+\delta,\uparrow}c_{i\uparrow} + \langle c^\dagger_{i+\delta,\uparrow}c_{i,\uparrow}\rangle c^\dagger_{i\downarrow}c_{i+\delta,\downarrow}\Big] \quad \text{(B.10)}$$

$$\text{HS} = -\frac{J}{4}\sum_{i\delta}\Big[\langle c^\dagger_{i\uparrow}c_{i\uparrow}\rangle c^\dagger_{i+\delta,\downarrow}c_{i+\delta,\downarrow} + \langle c^\dagger_{i+\delta,\downarrow}c_{i+\delta,\downarrow}\rangle c^\dagger_{i\uparrow}c_{i\uparrow} + \langle c^\dagger_{i\downarrow}c_{i\downarrow}\rangle c^\dagger_{i+\delta,\uparrow}c_{i+\delta,\uparrow} + \langle c^\dagger_{i+\delta,\uparrow}c_{i+\delta,\uparrow}\rangle c^\dagger_{i\downarrow}c_{i\downarrow}\Big] \quad \text{(B.11)}$$

$$C_{\text{shift}} = +\frac{J}{4}\sum_{i\delta}\Big[\langle c^\dagger_{i\uparrow}c_{i+\delta,\uparrow}\rangle\langle c^\dagger_{i+\delta,\downarrow}c_{i\downarrow}\rangle + \langle c^\dagger_{i\downarrow}c_{i+\delta,\uparrow}\rangle\langle c^\dagger_{i+\delta,\uparrow}c_{i\uparrow}\rangle + \langle c^\dagger_{i\uparrow}c_{i\uparrow}\rangle\langle c^\dagger_{i+\delta,\downarrow}c_{i+\delta,\downarrow}\rangle + \langle c^\dagger_{i\downarrow}c_{i\downarrow}\rangle\langle c^\dagger_{i+\delta,\uparrow}c_{i+\delta,\uparrow}\rangle\Big], \quad \text{(B.12)}$$

where H.C. is the Hermitian conjugate of the preceding operators.

For the pairing terms given by (B.8), if there is no triplet component then there can be no spin excess in the pairing mean-fields. That is, $\langle c_{j\downarrow}c_{i\uparrow}\rangle + \langle c_{j\uparrow}c_{i\downarrow}\rangle = 0$. From this relation, it follows that $\langle c_{j\downarrow}c_{i\uparrow}\rangle = -\langle c_{j\uparrow}c_{i\downarrow}\rangle$. Thus,

$$\begin{aligned}
\text{SC} &= -\frac{J}{4}\sum_{i\delta}\Big[\Big(\langle c_{i\downarrow}c_{i+\delta,\uparrow}\rangle + \langle c_{i+\delta,\downarrow}c_{i\uparrow}\rangle\Big)c^\dagger_{i\uparrow}c^\dagger_{i+\delta,\downarrow} + \Big(\langle c_{i+\delta,\uparrow}c_{i\downarrow}\rangle + \langle c_{i\uparrow}c_{i+\delta,\downarrow}\rangle\Big)c^\dagger_{i\downarrow}c^\dagger_{i+\delta,\uparrow} + \text{H.C.}\Big] \\
&= -\frac{J}{4}\sum_{i\delta}\Big[\Big(\langle c_{i\downarrow}c_{i+\delta,\uparrow}\rangle + \langle c_{i+\delta,\downarrow}c_{i\uparrow}\rangle\Big)c^\dagger_{i\uparrow}c^\dagger_{i+\delta,\downarrow} + \Big(\langle c_{i\downarrow}c_{i+\delta,\uparrow}\rangle + \langle c_{i+\delta,\downarrow}c_{i\uparrow}\rangle\Big)c^\dagger_{i+\delta,\uparrow}c^\dagger_{i\downarrow} + \text{H.C.}\Big] \\
&= -\frac{J}{4}\sum_{i\delta}\Big[\Big(\langle c_{i\downarrow}c_{i+\delta,\uparrow}\rangle + \langle c_{i+\delta,\downarrow}c_{i\uparrow}\rangle\Big)\Big(c^\dagger_{i\uparrow}c^\dagger_{i+\delta,\downarrow} + c^\dagger_{i+\delta,\uparrow}c^\dagger_{i\downarrow}\Big) + \text{H.C.}\Big] \\
&= \sum_{i\delta}\Big\{\Delta^\delta_i\left[c^\dagger_{i\uparrow}c^\dagger_{i+\delta,\downarrow} + c^\dagger_{i+\delta,\uparrow}c^\dagger_{i\downarrow}\right] + \text{H.C.}\Big\} \\
&= \sum_{i\delta\sigma}\Big\{\Delta^\delta_{i\sigma}c^\dagger_{i\sigma}c^\dagger_{i+\delta,-\sigma} + \text{H.C.}\Big\}, \qquad \text{(B.13)}
\end{aligned}$$

where the d-wave SC gap order parameter is therefore defined as

$$\Delta^\delta_{i\sigma} \equiv -\sigma\frac{J}{4}\big[\langle c_{i,-\sigma}c_{i+\delta,\sigma}\rangle + \langle c_{i+\delta,-\sigma}c_{i,\sigma}\rangle\big]. \quad \text{(B.14)}$$

Turning to the Hartree shift terms in (B.11),

$$\text{HS} = -\frac{J}{4}\sum_{i\delta}\Big[\langle n_{i\uparrow}\rangle n_{i+\delta,\downarrow} + \langle n_{i+\delta,\downarrow}\rangle n_{i\uparrow} + \langle n_{i\downarrow}\rangle n_{i+\delta,\uparrow} + \langle n_{i+\delta,\uparrow}\rangle n_{i\downarrow}\Big]. \quad \text{(B.15)}$$

Because the site indices on the individual terms in (B.15) can be switched with impunity, this expression can be re-cast in the following form:

$$\text{HS} = -\frac{J}{4}\sum_{i\delta}\Big[\langle n_{i+\delta,\downarrow}\rangle n_{i\uparrow} + \langle n_{i+\delta,\downarrow}\rangle n_{i\uparrow} + \langle n_{i+\delta,\uparrow}\rangle n_{i\downarrow} + \langle n_{i+\delta,\uparrow}\rangle n_{i\downarrow}\Big] \quad \text{(B.16)}$$

The total charge density ρ_i on site i is defined by

$$\rho_i \equiv \langle n_{i\uparrow}\rangle + \langle n_{i\downarrow}\rangle, \quad \text{(B.17)}$$

while the staggered antiferromagnetic (AF) magnetization m_i is defined by

$$\begin{aligned} m_i(-1)^{x_i+y_i} &\equiv \frac{1}{2}\big[\langle n_{i\uparrow}\rangle - \langle n_{i\downarrow}\rangle\big] \\ \Longrightarrow \quad m_i &= \frac{1}{2}\big[\langle n_{i\uparrow}\rangle - \langle n_{i\downarrow}\rangle\big] e^{i\mathbf{Q}_M\cdot\mathbf{r}_i}, \end{aligned} \tag{B.18}$$

where $\mathbf{r}_i = x_i\hat{\mathbf{x}} + y_i\hat{\mathbf{y}}$ is the position vector for site i, and $\mathbf{Q}_M = \pm\pi\hat{\mathbf{x}} \pm \pi\hat{\mathbf{y}}$ is the AF-ordering vector. Rearranging (B.18) and making use of (B.17), one finds that

$$\langle n_{i\sigma}\rangle = \frac{\rho_i}{2} + \sigma m_i e^{i\mathbf{Q}_M\cdot\mathbf{r}_i}. \tag{B.19}$$

Making use of this definition,

$$\langle n_{i+\delta,\uparrow}\rangle = \frac{\rho_{i+\delta}}{2} + m_{i+\delta}e^{i\mathbf{Q}\cdot\mathbf{r}_{i+\delta}}, \quad \langle n_{i+\delta,\downarrow}\rangle = \frac{\rho_{i+\delta}}{2} - m_{i+\delta}e^{i\mathbf{Q}\cdot\mathbf{r}_{i+\delta}}. \tag{B.20}$$

Then for (B.16),

$$\begin{aligned} \text{HS} &= -\frac{J}{4}(2)\sum_{i\delta}\left[\frac{\rho_{i+\delta}}{2}n_{i\downarrow} + m_{i+\delta}e^{i\mathbf{Q}\cdot\mathbf{r}_{i+\delta}}n_{i\downarrow} + \frac{\rho_{i+\delta}}{2}n_{i\uparrow} - m_{i+\delta}e^{i\mathbf{Q}\cdot\mathbf{r}_{i+\delta}}n_{i\uparrow}\right] \\ &= -\frac{J}{4}(2)\sum_{i\delta}\left[\frac{\rho_{i+\delta}}{2}\big(n_{i\uparrow}+n_{i\downarrow}\big) - m_{i+\delta}e^{i\mathbf{Q}\cdot\mathbf{r}_{i+\delta}}\big(n_{i\uparrow}-n_{i\downarrow}\big)\right] \\ &= -\frac{J}{4}\sum_{i\delta\sigma}\rho_{i+\delta}n_{i\sigma} + \frac{J}{2}\sum_{i\delta\sigma}\sigma m_{i+\delta}e^{i\mathbf{Q}\cdot\mathbf{r}_{i+\delta}}n_{i\sigma} \\ &= -\frac{J}{4}\sum_{i\delta\sigma}\rho_{i+\delta}n_{i\sigma} - \frac{J}{2}\sum_{i\delta\sigma}\sigma m_{i+\delta}e^{i\mathbf{Q}\cdot\mathbf{r}_{i}}n_{i\sigma}. \end{aligned} \tag{B.21}$$

The HS order parameter is therefore defined as

$$\eta_i \equiv -\frac{J}{4}\sum_{\delta}\rho_{i+\delta}, \tag{B.22}$$

and the AF order parameter is likewise defined as

$$M_i \equiv \frac{J}{2}\sum_{\delta} m_{i+\delta}. \tag{B.23}$$

Finally, for the Fock shift terms, consolidating (B.10) with the introduction of a

spin index gives

$$\begin{aligned} \text{FS} &= -\frac{J}{4}\sum_{i\delta\sigma}\left[\langle c^{\dagger}_{i,-\sigma}c_{i+\delta,-\sigma}\rangle c^{\dagger}_{i+\delta,\sigma}c_{i,\sigma} + \langle c^{\dagger}_{i+\delta,-\sigma}c_{i,-\sigma}\rangle c^{\dagger}_{i,\sigma}c_{i+\delta,\sigma}\right] \\ &= -\frac{J}{2}\sum_{i\delta\sigma}\langle c^{\dagger}_{i+\delta,-\sigma}c_{i,-\sigma}\rangle c^{\dagger}_{i,\sigma}c_{i+\delta,\sigma}, \end{aligned} \tag{B.24}$$

where the indices have been interchanged in the first term on going to the second line, allowing the two terms to be combined. From (B.24), the FS order parameter is defined as

$$\tau^{\delta}_{i\sigma} = \frac{J}{2}\langle c^{\dagger}_{i+\delta,-\sigma}c_{i,-\sigma}\rangle. \tag{B.25}$$

Combining equations (B.13); (B.16) with (B.22) and (B.23); and (B.24) with (B.25) all into the t-J Hamiltonian (3.3), the following effective Hamiltonian is arrived at:

$$\begin{aligned} H_{\text{eff}} \equiv & -\sum_{i\delta\sigma}\left(t+\tau^{\delta}_{i\sigma}\right)c^{\dagger}_{i\sigma}c_{i+\delta,\sigma} - \sum_{i\sigma}\left[\mu-\eta_i+\sigma M_i e^{i\mathbf{Q}_M\cdot\mathbf{r}_i}\right]n_{i\sigma} \\ & + \sum_{i\delta\sigma}\left\{\Delta^{\delta}_{i\sigma}\left[c^{\dagger}_{i,\sigma}c^{\dagger}_{i+\delta,-\sigma} + c^{\dagger}_{i+\delta,\sigma}c^{\dagger}_{i,-\sigma}\right] + \text{H.C.}\right\} + C, \end{aligned} \tag{B.26}$$

where

$$C \equiv C_{\text{shift}} + C_{\text{pair}}, \tag{B.27}$$

is the sum of all of the constant factorization terms emerging from the mean-field decomposition, and can be subtracted off of the effective Hamiltonian.

Appendix C

Self-Consistent Equations for the π-Striped Superconductor

The purpose of this appendix is to derive the self-consistent equations for the SC order parameter of the π-striped superconductor. Note that the self-consistent equations obtained from the t-J model in Section 3.1.1 for the Hartree and Fock shifts, as well as that for the filling, do not differ in structure because the SC order is modulated (however, the eigenvectors of the BdG equations which enter these equations will obviously be different). The method used to derive self-consistent equations for the π-striped SC order parameter is to Fourier transform the electron operators of both the SC part of the phenomenological, effective Hamiltonian (2.1) and the SC part of the effective Hamiltonian obtained from the mean-field decomposition of the t-J model. The coefficients of the resulting Fourier-transformed electron operator terms, which contain the information about the modulation of the SC order, can then be matched up between the two cases, in order to obtain an equation which connects the π-striped order parameter with the relevant microscopic Hamiltonian.

The Fourier-transformed electron operators are defined as

$$c_{\mathbf{k}\sigma} = \frac{1}{\sqrt{N}} \sum_{\mathbf{r}} e^{-i\mathbf{k}\cdot\mathbf{r}} c_{x,y,\sigma}, \qquad c_{x,y,\sigma} = \frac{1}{\sqrt{N}} \sum_{\mathbf{k}} e^{i\mathbf{k}\cdot\mathbf{r}} c_{\mathbf{k}\sigma}. \tag{C.1}$$

The Fourier transform of the SC part of (2.1) using (C.1) is given by

$$\begin{aligned} H'_{\text{eff}} \;=\; & \frac{1}{N} \sum_{xy} \sum_{\mathbf{k}\mathbf{k}'} e^{-i(k_x+k'_x)x} e^{-i(k_y+k'_y)y} \Big[\\ & \Delta \cos(Q_x x) \big(e^{-ik'_x a} + e^{-ik_x a}\big) c^\dagger_{\mathbf{k}\uparrow} c^\dagger_{\mathbf{k}'\downarrow} \\ & - \Delta \cos[Q_x(x-1/2)] \big(e^{-ik'_y a} + e^{-ik_y a}\big) c^\dagger_{\mathbf{k}\uparrow} c^\dagger_{\mathbf{k}'\downarrow} + \text{H.C.} \Big]. \end{aligned} \tag{C.2}$$

From (B.13), the SC part of the decomposed t-J Hamiltonian, after some algebra,

can be rewritten as

$$H'_{\mathrm{tJ}} = -\frac{J}{2}\sum_{xy}\Big[\Big(\langle c_{x,y,\downarrow}c_{x+1,y,\uparrow}\rangle + \langle c_{x+1,y,\downarrow}c_{x,y,\uparrow}\rangle\Big)\Big(c^{\dagger}_{x,y,\uparrow}c^{\dagger}_{x+1,y,\downarrow} + c^{\dagger}_{x+1,y,\uparrow}c^{\dagger}_{x,y,\downarrow}\Big) + \Big(\langle c_{x,y,\downarrow}c_{x,y+1,\uparrow}\rangle + \langle c_{x,y+1,\downarrow}c_{x,y,\uparrow}\rangle\Big)\Big(c^{\dagger}_{x,y,\uparrow}c^{\dagger}_{x,y+1,\downarrow} + c^{\dagger}_{x,y+1,\uparrow}c^{\dagger}_{x,y,\downarrow}\Big) + \mathrm{H.C.}\Big]. \tag{C.3}$$

The Fourier-transformed expression is

$$\begin{aligned} H'_{\mathrm{tJ}} = -\frac{J}{2N^2}\sum_{xy}\sum_{\mathbf{kk'}}\sum_{\mathbf{qq'}} e^{-i(k_x+k'_x)x}e^{-i(k_y+k'_y y)}\Big[& \\ & e^{i(q_x+q'_x)x}e^{i(q_y+q'_y)y}\big(e^{iq'_x a}+e^{iq_x a}\big)\big(e^{-ik'_x a}+e^{-ik_x a}\big)\langle c_{\mathbf{q}\downarrow}c_{\mathbf{q'}\uparrow}\rangle c^{\dagger}_{\mathbf{k}\uparrow}c^{\dagger}_{\mathbf{k'}\downarrow} \\ + \; & e^{i(q_x+q'_x)x}e^{i(q_y+q'_y)y}\big(e^{iq'_y a}+e^{iq_y a}\big)\big(e^{-ik'_y a}+e^{-ik_y a}\big)\langle c_{\mathbf{q}\downarrow}c_{\mathbf{q'}\uparrow}\rangle c^{\dagger}_{\mathbf{k}\uparrow}c^{\dagger}_{\mathbf{k'}\downarrow} \\ + \; & \mathrm{H.C.}\Big]. \end{aligned} \tag{C.4}$$

Comparing the first terms of (C.2) and (C.4), it must be that

$$\begin{aligned} \Delta\Big(\frac{e^{iQ_x x}+e^{-iQ_x x}}{2}\Big) = -\frac{J}{2N}\sum_{\mathbf{qq'}}\Big[& e^{i(q_x+q'_x)x}e^{i(q_y+q'_y)y}e^{iq'_x a}\langle c_{\mathbf{q}\downarrow}c_{\mathbf{q'}\uparrow}\rangle \\ & + \; e^{i(q_x+q'_x)x}e^{i(q_y+q'_y)y}e^{iq_x a}\langle c_{\mathbf{q}\downarrow}c_{\mathbf{q'}\uparrow}\rangle\Big]. \end{aligned} \tag{C.5}$$

In order for this equality to hold, the spatial dependence must be identical on both sides, which implies that $q'_x = -q_x \pm Q_x$ and $q'_y = -q_y$ (for all other terms in the $\mathbf{q}'$ sum, it must therefore be the case that $\langle c_{\mathbf{q}\downarrow}c_{\mathbf{q'}\uparrow}\rangle = 0$). Two mutually exclusive cases then emerge, for each of the two terms on the right-hand side of (C.5):[1]

$$\Delta e^{\pm iQ_x x} = -\frac{J}{N}\sum_{\mathbf{qq'}} e^{i(q_x+q'_x)x}e^{i(q_y+q'_y)y}e^{iq'_x a}\langle c_{\mathbf{q},\downarrow}c_{\mathbf{q'}\uparrow}\rangle\delta_{\mathbf{q'},-\mathbf{q}\pm Q_x\hat{x}}, \tag{C.6}$$

and

$$\Delta e^{\mp iQ_x x} = -\frac{J}{N}\sum_{\mathbf{qq'}} e^{i(q_x+q'_x)x}e^{i(q_y+q'_y)y}e^{iq_x a}\langle c_{\mathbf{q}\downarrow}c_{\mathbf{q'}\uparrow}\rangle\delta_{\mathbf{q'},-\mathbf{q}\mp Q_x\hat{x}}. \tag{C.7}$$

On performing the $\mathbf{q}'$ sums, the result is that

$$\Delta = -\frac{J}{N}\sum_{\mathbf{q}} e^{\pm iQ_x a}e^{-iq_x a}\langle c_{\mathbf{q}\downarrow}c_{-\mathbf{q}\pm Q_x\hat{x},\uparrow}\rangle \tag{C.8}$$

$$\Delta = -\frac{J}{N}\sum_{\mathbf{q}} e^{iq_x a}\langle c_{\mathbf{q},\downarrow}c_{-\mathbf{q}\mp Q_x\hat{x},\uparrow}\rangle. \tag{C.9}$$

Adding together the corresponding cases from (C.8) and (C.9) and halving the result,

[1] If the first expression has the upper ± sign, then so too must the second expression.

two distinct representations of Δ from the x-direction pairing are obtained:[2]

$$\Delta^{\hat{x}} = -\frac{J}{2N}\sum_{\mathbf{q}}\Big[e^{-iq_x a}e^{iQ_x x}\langle c_{\mathbf{q},\downarrow}c_{-\mathbf{q}+Q_x\hat{x},\uparrow}\rangle + e^{iq_x a}\langle c_{\mathbf{q},\downarrow}c_{-\mathbf{q}-Q_x\hat{x},\uparrow}\rangle\Big] \tag{C.10}$$

$$\Delta^{\hat{x}} = -\frac{J}{2N}\sum_{\mathbf{q}}\Big[e^{-iq_x a}e^{-iQ_x a}\langle c_{\mathbf{q},\downarrow}c_{-\mathbf{q}-Q_x\hat{x},\uparrow}\rangle + e^{iq_x a}\langle c_{\mathbf{q},\downarrow}c_{-\mathbf{q}+Q_x\hat{x},\uparrow}\rangle\Big]. \tag{C.11}$$

Going through the same process for the y-direction pairing, the second terms in equations (C.2) and (C.4) give:

$$\Delta^{\hat{y}} = \frac{J}{2N}\sum_{\mathbf{q}}\Big[e^{-iq_y a}e^{iQ_x a/2}\langle c_{\mathbf{q},\downarrow}c_{-\mathbf{q}+Q_x\hat{x},\uparrow}\rangle + e^{iq_y a}e^{-iQ_x a/2}\langle c_{\mathbf{q},\downarrow}c_{-\mathbf{q}-Q_x\hat{x},\uparrow}\rangle\Big] \tag{C.12}$$

$$\Delta^{\hat{y}} = \frac{J}{2N}\sum_{\mathbf{q}}\Big[e^{-iq_y a}e^{-iQ_x a/2}\langle c_{\mathbf{q},\downarrow}c_{-\mathbf{q}-Q_x\hat{x},\uparrow}\rangle + e^{iq_y a}e^{iQ_x a/2}\langle c_{\mathbf{q},\downarrow}c_{-\mathbf{q}+Q_x\hat{x},\uparrow}\rangle\Big]. \tag{C.13}$$

Having extracted the bond-centred cosine modulation from the ordinary d-wave SC order parameter originating from the decoupled t-J Hamiltonian, the operators can now be transformed back to their real-space representations, so that the order parameter can be calculated directly from the real-space BdG wavefunction emerging from the code (since the code uses the real-space effective Hamiltonian (2.1) to construct the BdG equations within a unit cell). From (C.10),

$$\begin{aligned}\Delta^{\hat{x}} \;=\; -\frac{J}{2N^2}\sum_{\mathbf{q}}\sum_{\mathbf{r}\mathbf{r}'}\Big[&e^{-iq_x(x-x'+a)}e^{-iq_y(y-y')}e^{iQ_x a}e^{-iQ_x x'}\langle c_{x,y,\downarrow}c_{x',y',\uparrow}\rangle \\ &+\; e^{-iq_x(x-x'-a)}e^{-iq_y(y-y')}e^{iQ_x x'}\langle c_{x,y,\downarrow}c_{x',y',\uparrow}\rangle\Big].\end{aligned} \tag{C.14}$$

Completing the sum over $\mathbf{q}$,

$$\begin{aligned}\Delta^{\hat{x}} \;&=\; -\frac{J}{2N^2}\sum_{\mathbf{r}\mathbf{r}'}\Big[e^{iQ_x a}e^{-iQ_x x'}\langle c_{x,y,\downarrow}c_{x',y',\uparrow}\rangle N_x\delta_{x',x+a}N_y\delta_{y',y} + e^{iQ_x x'}\langle c_{x,y,\downarrow}c_{x',y',\uparrow}\rangle N_x\delta_{x',x-1}N_y\delta_{y',y}\Big] \\ &=\; -\frac{J}{2N}\sum_{\mathbf{r}}\Big[e^{-iQ_x x}\langle c_{x,y,\downarrow}c_{x+1,y,\uparrow}\rangle + e^{iQ_x x}e^{-iQ_x a}\langle c_{x,y,\downarrow}c_{x-1,y,\uparrow}\rangle\Big].\end{aligned} \tag{C.15}$$

By a relabeling of the indices in the second term,[3] the result is that

$$\Delta^{\hat{x}} = -\frac{J}{2N}\sum_{\mathbf{r}}\Big[e^{-iQ_x x}\langle c_{x,y,\downarrow}c_{x+1,y,\uparrow}\rangle + e^{iQ_x x}\langle c_{x+1,y,\downarrow}c_{x,y,\uparrow}\rangle\Big]. \tag{C.16}$$

Similarly, inverting the Fourier transform for the second of the $\Delta^{\hat{x}}$ expressions (C.11),

[2] That these terms derive from pairing in the x-direction is reflected in the addition of a book-keeping superscript, to differentiate from the forthcoming y-direction expressions.

[3] $x \to x + a$, which is permissible under the assumption of Born-von Karman boundary conditions.

the same expression is obtained, but with the phases conjugated:

$$\Delta^{\hat{x}} = -\frac{J}{2N}\sum_{\mathbf{r}}\left[e^{iQ_x x}\langle c_{x,y,\downarrow}c_{x+1,y,\uparrow}\rangle + e^{-iQ_x x}\langle c_{x+1,y,\downarrow}c_{x,y,\uparrow}\rangle\right]. \tag{C.17}$$

Clearly, equations (C.16) and (C.17) can be combined and the exponentials can be re-expressed as a cosine:

$$\Delta^{\hat{x}} = -\frac{J}{2N}\sum_{x,y}\cos\left(Q_x x\right)\left[\langle c_{x,y,\downarrow}c_{x+1,y,\uparrow}\rangle + \langle c_{x+1,y,\downarrow}c_{x,y,\uparrow}\rangle\right]. \tag{C.18}$$

This produces an expression which reduces to the self-consistent equation for the uniform d-wave case when $Q_x = 0$, since in that case it would be the average over all sites of a uniform quantity, *i.e.* the uniform value of $\Delta^{\hat{x}}$ at each bond.[4] Working through the same process for the $\Delta^{\hat{y}}$ expressions contained in equations (C.12) and (C.13), the equivalent expression can be constructed from the pairing expectation values in the y-direction:

$$\Delta^{\hat{y}} = \frac{J}{2N}\sum_{x,y}\cos\left[Q_x(x-1/2)\right]\left[\langle c_{x,y,\downarrow}c_{x,y+1,\uparrow}\rangle + \langle c_{x,y+1,\downarrow}c_{x,y,\uparrow}\rangle\right]. \tag{C.19}$$

Since $\Delta^{\hat{x}}$ and $\Delta^{\hat{y}}$ actually represent the same quantity, it is natural to combine both of these expressions into a single SC order parameter for the π-striped SC:

$$\begin{aligned}\Delta \;=\; -\frac{J}{4N}\sum_{x,y}\Big\{ &\cos\left(Q_x x\right)\left[\langle c_{x,y,\downarrow}c_{x+1,y,\uparrow}\rangle + \langle c_{x+1,y,\downarrow}c_{x,y,\uparrow}\rangle\right] \\ &- \cos\left[Q_x(x-1/2)\right]\left[\langle c_{x,y,\downarrow}c_{x,y+1,\uparrow}\rangle + \langle c_{x,y+1,\downarrow}c_{x,y,\uparrow}\rangle\right]\Big\}.\end{aligned} \tag{C.20}$$

Equation (C.20) makes the BdG equations (2.7) for the π-striped SC self-consistent.

[4] Note that the reduction is up to a factor of 2, which is present in the uniform case BdG equations, but not in the π-striped case, owing to a difference in how the respective effective Hamiltonians are defined. In the same way, the sign difference between the x- and y-direction SC gap is explicit in the π-striped effective Hamiltonian, but not in that for the uniform case.

Bibliography

A. S. Alexandrov. Theory of quantum magneto-oscillations in underdoped cuprate superconductors. *Journal of Physics: Condensed Matter*, 20(19):192202, 2008.

P. Anderson. The resonating valence bond state in La_2CuO_4 and superconductivity. *Science*, 235(4793):1196–1198, 1987.

N. W. Ashcroft and N. D. Mermin. *Solid State Physics*. Brooks/Cole, Belmont, CA, 1976.

A. F. Bangura, J. D. Fletcher, A. Carrington, J. Levallois, M. Nardone, B. Vignolle, P. J. Heard, N. Doiron-Leyraud, D. LeBoeuf, L. Taillefer, S. Adachi, C. Proust, and N. E. Hussey. Small Fermi surface pockets in underdoped high temperature superconductors: Observation of Shubnikov–de Haas oscillations in $YBa_2Cu_4O_8$. *Phys. Rev. Lett.*, 100:047004, Feb 2008.

S. Baruch and D. Orgad. Spectral signatures of modulated d-wave superconducting phases. *Phys. Rev. B*, 77:174502, May 2008.

D. Basov and A. Chubukov. Manifesto for a higher T_c. *Nat. Phys.*, 7:272–276, Apr 2011.

J. Bednorz and K. Müller. Possible high-T_c superconductivity in the Ba–La–Cu–O system. *Zeitschrift für Physik B Condensed Matter*, 64(2):189–193, 1986. ISSN 0722-3277.

E. Berg, E. Fradkin, E.-A. Kim, S. A. Kivelson, V. Oganesyan, J. M. Tranquada, and S. C. Zhang. Dynamical layer decoupling in a stripe-ordered high-T_c superconductor. *Phys. Rev. Lett.*, 99:127003, Sep 2007.

E. Berg, E. Fradkin, and S. A. Kivelson. Theory of the striped superconductor. *Phys. Rev. B*, 79:064515, Feb 2009.

S. V. Borisenko, A. A. Kordyuk, A. N. Yaresko, V. B. Zabolotnyy, D. S. Inosov, R. Schuster, B. Büchner, R. Weber, R. Follath, L. Patthey, and H. Berger. Pseudogap and charge density waves in two dimensions. *Phys. Rev. Lett.*, 100:196402, May 2008.

E. Brown. Bloch electrons in a uniform magnetic field. *Phys. Rev.*, 133:A1038–A1044, Feb 1964.

E. Dagotto. Correlated electrons in high-temperature superconductors. *Rev. Mod. Phys.*, 66:763–840, Jul 1994.

A. Damascelli, Z. Hussain, and Z.-X. Shen. Angle-resolved photoemission studies of the cuprate superconductors. *Rev. Mod. Phys.*, 75:473–541, Apr 2003.

P. de Gennes. *Superconductivity of Metals and Alloy*. Westview Press, 1966.

N. Doiron-Leyraud, C. Proust, D. LeBoeuf, J. Levallois, J.-B. Bonnemaison, R. Liang, D. Bonn, W. Hardy, and L. Taillefer. Quantum oscillations and the Fermi surface in an underdoped high-T_c superconductor. *Nature*, 447:565–568, May 2007.

I. S. Elfimov, G. A. Sawatzky, and A. Damascelli. Theory of fermi-surface pockets and correlation effects in underdoped $YBa_2Cu_3O_{6.5}$. *Phys. Rev. B*, 77:060504, Feb 2008.

A. Ghosal, C. Kallin, and A. J. Berlinsky. Competition of superconductivity and antiferromagnetism in a d-wave vortex lattice. *Phys. Rev. B*, 66:214502, Dec 2002.

C. Gros, R. Joynt, and T. M. Rice. Antiferromagnetic correlations in almost-localized Fermi liquids. *Phys. Rev. B*, 36:381–393, Jul 1987.

N. Harrison. Spin-density wave Fermi surface reconstruction in underdoped $YBa_2Cu_3\mathbf{O}_{6+x}$. *Phys. Rev. Lett.*, 102:206405, May 2009.

A. Himeda, T. Kato, and M. Ogata. Stripe states with spatially oscillating d-wave superconductivity in the two-dimensional t-t'-J model. *Phys. Rev. Lett.*, 88:117001, Feb 2002.

J. Hubbard. Electron correlations in narrow energy bands. *Proceedings of the Royal Society of London. Series A. Mathematical and Physical Sciences*, 276(1365):238–257, 1963.

C. Jaudet, D. Vignolles, A. Audouard, J. Levallois, D. LeBoeuf, N. Doiron-Leyraud, B. Vignolle, M. Nardone, A. Zitouni, R. Liang, D. A. Bonn, W. N. Hardy, L. Taillefer, and C. Proust. de Haas–van Alphen oscillations in the underdoped high-temperature superconductor $YBa_2Cu_3O_{6.5}$. *Phys. Rev. Lett.*, 100:187005, May 2008.

C. Jayaprakash, H. R. Krishnamurthy, and S. Sarker. Mean-field theory for the t-J model. *Phys. Rev. B*, 40:2610–2613, Aug 1989.

A. Kanigel, M. R. Norman, M. Randeria, U. Chatterjee, S. Souma, A. Kaminski, H. M. Fretwell, S. Rosenkranz, M. Shi, T. Sato, T. Takahashi, Z. Z. Li, H. Raffy, K. Kadowaki, D. Hinks, L. Ozyuzer, and J. C. Campuzano. Evolution of the pseudogap from Fermi arcs to the nodal liquid. *Nat. Phys.*, 2:447–451, Jul 2006.

D. Knapp. *Studies of the Vortex State in High-Temperature Superconductors*. McMaster University, Hamilton, Ontario, 2005.

D. Knapp, C. Kallin, A. Ghosal, and S. Mansour. Antiferromagnetism and charged vortices in high-T_c superconductors. *Phys. Rev. B*, 71:064504, Feb 2005.

D. LeBoeuf, N. Doiron-Leyraud, J. Levallois, R. Daou, J.-B. Bonnemaison, N. Hussey, L. Balicas, B. Ramshaw, R. Liang, D. Bonn, W. Hardy, S. Adachi, C. Proust, and L. Taillefer. Electron pockets in the Fermi surface of hole-doped high-T_c superconductors. *Nature*, 450:533–536, Nov 2007.

P. A. Lee, N. Nagaosa, and X.-G. Wen. Doping a Mott insulator: Physics of high-temperature superconductivity. *Rev. Mod. Phys.*, 78:17–85, Jan 2006.

A. J. Millis and M. R. Norman. Antiphase stripe order as the origin of electron pockets observed in 1/8-hole-doped cuprates. *Phys. Rev. B*, 76:220503, Dec 2007.

M. Norman. Have cuprates earned their stripes? *Science*, 303(5666):1985–1986, 2004.

M. Norman and C. Pépin. The electronic nature of high temperature cuprate superconductors. *Reports on Progress in Physics*, 66(10):1547, 2003.

M. Ogata and H. Fukuyama. The t-J model for the oxide high-T_c superconductors. *Rev. Prog. Phys.*, 71:036501, March 2008.

L. Onsager. Interpretation of the de Haas–van Alphen effect. *Philosophical Magazine Series 7*, 43(344):1006–1008, 1952.

J. Orenstein and A. J. Millis. Advances in the physics of high-temperature superconductivity. *Science*, 288(5465):468–474, 2000.

C. V. Parker, P. Aynajian, E. H. da Silva Neto, A. Pushp, S. Ono, J. Wen, Z. Xu, G. Gu, and A. Yazdani. Fluctuating stripes at the onset of the pseudogap in the high-T_c superconductor $Bi_2Sr_2CaCu_2O_{8+x}$. *Nature*, 468:677–680, Dec 2010.

T. Pereg-Barnea, H. Weber, G. Refael, and M. Franz. Quantum oscillations from Fermi arcs. *Nat. Phys.*, 6:44–49, Jan 2010.

D. Podolsky, E. Demler, K. Damle, and B. I. Halperin. Translational symmetry breaking in the superconducting state of the cuprates: Analysis of the quasiparticle density of states. *Phys. Rev. B*, 67:094514, Mar 2003.

M. Raczkowski, M. Capello, D. Poilblanc, R. Frésard, and A. M. Oleś. Unidirectional d-wave superconducting domains in the two-dimensional t-J model. *Phys. Rev. B*, 76:140505, Oct 2007.

M. Randeria, J.-M. Duan, and L.-Y. Shieh. Bound states, Cooper pairing, and Bose condensation in two dimensions. *Phys. Rev. Lett.*, 62:981–984, Feb 1989.

S. Riggs, O. Vafek, J. Kemper, J. Betts, A. Migliori, F. Balakirev, W. Hardy, R. Liang, D. Bonn, and G. Boebinger. Heat capacity through the magnetic-field-induced resistive transition in an underdoped high-temperature superconductor. *Nat. Phys.*, 7:332–335, Apr 2011.

P. M. C. Rourke, A. F. Bangura, C. Proust, J. Levallois, N. Doiron-Leyraud, D. LeBoeuf, L. Taillefer, S. Adachi, M. L. Sutherland, and N. E. Hussey. Fermi-surface reconstruction and two-carrier model for the Hall effect in $YBa_2Cu_4O_8$. *Phys. Rev. B*, 82:020514, Jul 2010.

D. J. Scalapino. A common thread: The pairing interaction for unconventional superconductors. *Rev. Mod. Phys.*, 84:1383–1417, Oct 2012.

S. Sebastian, N. Harrison, E. Palm, T. Murphy, C. Mielke, R. Liang, D. Bonn, W. Hardy, , and G. Lonzarich. A multi-component Fermi surface in the vortex state of an underdoped high-T_c superconductor. *Nature*, 454:200–203, Jul 2008.

J. Singleton, C. de la Cruz, R. D. McDonald, S. Li, M. Altarawneh, P. Goddard, I. Franke, D. Rickel, C. H. Mielke, X. Yao, and P. Dai. Magnetic quantum oscillations in $YBa_2Cu_3\mathbf{O}_{6.61}$ and $YBa_2Cu_3\mathbf{O}_{6.69}$ in fields of up to 85 T: Patching the hole in the roof of the superconducting dome. *Phys. Rev. Lett.*, 104:086403, Feb 2010.

Z. Tesanovic. The mystery and the mystique. *Nat. Phys.*, 7:283–284, Apr 2011.

T. Timusk and B. Statt. The pseudogap in high-temperature superconductors: an experimental survey. *Reports on Progress in Physics*, 62(1):61, 1999.

M. Tinkham. *Introduction to Superconductivity*. Dover Publications, Inc., Mineola, NY, 2004.

J. Tranquada, B. Sternlieb, J. Axe, Y. Nakamura, and S. Uchida. Evidence for stripe correlations of spins and holes in copper oxide superconductors. *Nature*, 375:561–563, Jun 1995.

C. C. Tsuei and J. R. Kirtley. Pairing symmetry in cuprate superconductors. *Rev. Mod. Phys.*, 72:969–1016, Oct 2000.

G. V. M. Williams, J. L. Tallon, E. M. Haines, R. Michalak, and R. Dupree. NMR evidence for a *d*-wave normal-state pseudogap. *Phys. Rev. Lett.*, 78:721–724, Jan 1997.

H. Yao, D.-H. Lee, and S. Kivelson. Fermi-surface reconstruction in a smectic phase of a high-temperature superconductor. *Phys. Rev. B*, 84:012507, Jul 2011.

E. A. Yelland, J. Singleton, C. H. Mielke, N. Harrison, F. F. Balakirev, B. Dabrowski, and J. R. Cooper. Quantum oscillations in the underdoped cuprate $YBa_2Cu_4O_8$. *Phys. Rev. Lett.*, 100:047003, Feb 2008.

J. Zak. Magnetic Translation Group. *Phys. Rev.*, 134:A1602–A1606, Jun 1964a.

J. Zak. Magnetic Translation Group. II. Irreducible Representations. *Phys. Rev.*, 134: A1607–A1611, Jun 1964b.

M. Zelli, C. Kallin, and A. J. Berlinsky. Mixed state of a π-striped superconductor. *Phys. Rev. B*, 84:174525, Nov 2011.

M. Zelli, C. Kallin, and A. J. Berlinsky. Quantum oscillations in a π-striped superconductor. *Phys. Rev. B*, 86:104507, Sep 2012.

F. C. Zhang and T. M. Rice. Effective Hamiltonian for the superconducting Cu oxides. *Phys. Rev. B*, 37:3759–3761, Mar 1988.

J. Zhou, J. Guo, H. Jiang, and J. Li. Spin dynamics in the stripe phase of high-T_c cuprates with the modulation of superconducting order. *The European Physical Journal B*, 82(3-4):295–301, 2011. ISSN 1434-6028.